

# Magnetic fields and differential rotation on the pre-main sequence I: The early-G star HD 141943 - brightness and magnetic topologies

S. C. Marsden,<sup>1,2\*</sup> M. M. Jardine,<sup>3\*</sup> J. C. Ramírez Vélez,<sup>4,5\*</sup> E. Alecian,<sup>4,6\*</sup>  
 C. J. Brown,<sup>7\*</sup> B. D. Carter,<sup>7\*</sup> J.-F. Donati,<sup>8\*</sup> N. Dunstone,<sup>3\*</sup> R. Hart,<sup>7\*</sup>  
 M. Semel<sup>4\*</sup> and I. A. Waite<sup>7\*</sup>

<sup>1</sup>Centre for Astronomy, School of Engineering and Physical Sciences, James Cook University, Townsville, 4811, Australia

<sup>2</sup>Australian Astronomical Observatory, PO Box 296, Epping NSW 1710, Australia

<sup>3</sup>SUPA, School of Physics and Astronomy, University of St. Andrews, St. Andrews, KY 16 9SS, Scotland

<sup>4</sup>LESIA, Observatoire de Paris-Meudon, F-92195 Meudon Cedex, France

<sup>5</sup>Instituto de Astronomía, Universidad Nacional Autónoma de México, 04510, Coyoacan, México D.F.

<sup>6</sup>LAOG, Laboratoire d'Astrophysique de Grenoble, Université Joseph Fourier, BP 53 38041, Grenoble Cedex 09, France

<sup>7</sup>Faculty of Sciences, University of Southern Queensland, Toowoomba, 4350, Australia

<sup>8</sup>LATT-UMR 5572, CNRS & Univ. de Toulouse, 14 Av. E. Belin, F-31400 Toulouse, France

Accepted version

## ABSTRACT

Spectroscopic and spectropolarimetric observations of the pre-main sequence early-G star HD 141943 were obtained at four observing epochs (in 2006, 2007, 2009 and 2010). The observations were undertaken at the 3.9-m Anglo-Australian Telescope using the UCLES echelle spectrograph and the SEMPOL spectropolarimeter visitor instrument. Brightness and surface magnetic field topologies were reconstructed for the star using the technique of least-squares deconvolution to increase the signal-to-noise of the data.

The reconstructed brightness maps show that HD 141943 had a weak polar spot and a significant amount of low latitude features, with little change in the latitude distribution of the spots over the 4 years of observations. The surface magnetic field was reconstructed at three of the epochs from a high order ( $l \leq 30$ ) spherical harmonic expansion of the spectropolarimetric observations. The reconstructed magnetic topologies show that in 2007 and 2010 the surface magnetic field was reasonably balanced between poloidal and toroidal components. However we find tentative evidence of a change in the poloidal/toroidal ratio in 2009 with the poloidal component becoming more dominant. At all epochs the radial magnetic field is predominantly non-axisymmetric while the azimuthal field is predominantly axisymmetric with a ring of positive azimuthal field around the pole similar to that seen on other active stars.

**Key words:** line : profiles – Stars : activity – imaging – magnetic fields – Stars : individual : HD 141943 – starspots

## 1 INTRODUCTION

The generation of magnetic fields is arguably one of the most important process operating inside a star affecting ev-

erything from the angular momentum evolution of the star through to the habitability of any planets around the star. In the solar case the magnetic dynamo is believed to operate in an interface layer between the differentially rotating convective zone and the radiative zone which rotates as a solid-body (Parker et al. 1993). However, for young, rapidly-rotating solar-type stars evidence is growing that such stars may in fact have a different dynamo mechanism. It has been suggested (Donati et al. 2003) that such stars may in fact house distributed dynamos, i.e. dynamos which operate across the entire convective zone, rather than be-

\* Email: Stephen.Marsden@jcu.edu.au (SCM); mmj@st-and.ac.uk (MMJ); jramirez@astroscu.unam.mx (JCRV); evelyne.alecian@obs.ujf-grenoble.fr (EA); brownca@usq.edu.au (CJB); carterb@usq.edu.au (BDC); donati@obs-mip.fr (J-FD); n.j.dunstone@googlemail.com (ND); rhodes.hart@usq.edu.au (RH); Meir.Semel@obspm.fr (MS); waite@usq.edu.au (IAW)

ing restricted to the interface-layer as in the solar case. The strongest evidence for this are large regions of near-surface azimuthal magnetic field seen on such stars (i.e. Donati et al. 2003; Marsden et al. 2006a). Such regions are believed to be the near-surface toroidal components of the large-scale dynamo field. In a solar-like interface-layer dynamo such fields should not be seen near the stellar surface and thus it is postulated that a distributed dynamo is operating in young, rapidly-rotating solar-type stars.

Most current dynamo models are based on our understanding of the Sun and are tailored to reproduce solar observations (see Parker et al. 1993; Charbonneau 2005). Such models usually involve an interface layer dynamo which, as discussed, may not apply to young solar-type stars, but there are some different dynamo models that have been examined. For example, the dynamo operating in fully convective stars (i.e. Browning 2008), or near-surface dynamos (i.e. Brandenburg 2005) or rapidly-rotating solar models with no interface layer (i.e. Brown et al. 2010). Still the operation of stellar magnetic dynamos is not well understood.

One of the most direct ways of observing the stellar dynamo is through the observation of the global magnetic field on the surface of a star. Zeeman Doppler imaging (ZDI, Semel 1989; Donati & Brown 1997) has been used for a number of years now to observe the magnetic field configurations of solar-type stars (i.e. Donati et al. 1992, 1999; Donati & Collier Cameron 1997; Donati 1999; Petit et al. 2004a,b, 2008; Marsden et al. 2006a; Jeffers & Donati 2008; Dunstone et al. 2008) and there is now a growing body of observations of the surface topologies of other stars that any stellar dynamo models needs to be able to reproduce.

Donati & Landstreet (2009) have summarised many of the observations of the magnetic fields of non-degenerate stars and for young solar-type stars (i.e. those with Rossby numbers  $\lesssim 1$  and more massive than  $\sim 0.5 M_{\odot}$ ) they find that these stars produce substantial toroidal fields and have mostly non-axisymmetric poloidal fields. For more mature stars, Petit et al. (2008) have shown that for solar-type stars with rotation periods faster than  $\sim 12$  days the global magnetic field of the star appears to be dominated by toroidal field with poloidal field being by far the most dominant field configuration for stars with slower rotation rates. This could indicate a change in the dynamo mechanism for solar-type stars rotating faster than  $\sim 12$  days. Such observations have yet to be modelled in stellar dynamo theory.

Doppler images of the surface spot topology of young solar-type stars show that they almost universally have large polar spot features (i.e. Barnes et al. 2000, 2001a,b; Donati et al. 2003; Marsden et al. 2005b, 2006a). This is in contrast to the predictions of current dynamo theory (i.e. Schussler et al. 1996; Granzer et al. 2000; Granzer 2004) and it has been suggested that a strong meridional flow may be responsible for transporting these spots from their emergence latitudes to the polar regions. This may also explain the mixed polarity of magnetic fields seen on the polar regions of many stars (see Mackay et al. 2004).

Although great progress has been made, our knowledge of stellar magnetic dynamos is still in its infancy. How the operation of the stellar magnetic dynamo depends on basic stellar parameters such as age, mass and rotation rate is still unknown.

One of the most obvious effects of the solar dy-

namo is the reversal of the Sun's global magnetic topology every  $\sim 11$  years, but so far only two other solar-type stars have shown evidence of global magnetic polarity reversals, HD 190771 (Petit et al. 2009) and Tau Boo (Donati et al. 2008; Fares et al. 2009). No strong evidence for a global polarity reversal has yet been seen on a young solar-type star, even though some, for example AB Dor (Donati & Collier Cameron 1997; Donati et al. 1999, 2003) have been observed for a number of years. Thus it is still unknown if young solar-type stars undergo regular magnetic cycles like the Sun or have chaotic cycles, as indicated by the Calcium HK emission of young stars (Baliunas et al. 1995).

For young solar-type stars the available spectropolarimetric observations are mainly of K-stars (i.e. Donati et al. 2003). At present there is only one young early-G star for which spectropolarimetric observations have been published in a refereed journal, HD 171488 (Marsden et al. 2006a; Jeffers & Donati 2008; Jeffers et al. 2010), with preliminary results for the late-F star HR 1817 (Mengel 2006; Marsden et al. 2006b, 2010a) being published as conference proceedings.

As part of a study into the magnetic topology and cycles of young late-F/early-G stars this paper along with that of Marsden et al. (2010b, Paper II) and Waite et al. (2010), presents spectropolarimetric observations of two early-G pre-main sequence (PMS) stars. This paper and Paper II deals with the observations of the young early-G star HD 141943, while the Waite et al. (2010) paper deals with observations of the similarly aged but more massive HD 106506.

HD 141943 was first identified by Waite et al. (2005) as a potential target for spectropolarimetric observations. It is active ( $\text{Log}(L_X) = 30.7 \text{ erg s}^{-1}$ , Cutispoto et al. 2002) and bright ( $V = 7.9$ , Cutispoto et al. 2002). It also has a very strong Lithium line ( $A_{\text{Li}} = 3.3$ , Cutispoto et al. 2003) indicating its youth ( $\sim 15$  Myrs, Cutispoto et al. 2003) and it is what we class as a moderately rapid rotator with a  $v \sin i \sim 38 \text{ km s}^{-1}$  (Cutispoto et al. 2003) and a period of  $2.20 \pm 0.03$  days (Cutispoto et al. 1999). According to Hillenbrand et al. (2008) HD 141943 is also possibly host to a  $\sim 85$  K debris disk.

This paper (Paper I) describes the evolution in both the brightness (reconstructed at 4 epochs) and magnetic (reconstructed at 3 epochs) topologies of HD 141943 taken at the Anglo-Australian telescope (AAT). A further paper on HD 141943 (Paper II) discusses the differential rotation,  $H\alpha$  emission and coronal magnetic field maps reconstructed from these observations.

## 2 OBSERVATIONS AND DATA REDUCTION

HD141943 was observed at 4 epochs on the 3.9-m AAT, in May 2006, March/April 2007, April 2009 and March/April 2010. The May 2006 observations were standard spectroscopic observations taken over a 6 night period using the University College London Echelle Spectrograph (UCLES). The 2007, 2009 and 2010 observations were spectropolarimetric, observing both left- and right-hand circularly polarised light using the SEMPOL (or SEMELPOL) spectropolarimeter (Semel, Donati & Rees 1993; Donati et al. 2003) visitor instrument in conjunction with UCLES. The observations in 2007, 2009 and 2010 were taken over 11, 7

and 12 nights respectively. A log of the observations is given in Table 1. The rotational phase of the observations was determined from the following ephemeris:

$$\text{HJD} = 2454195.154 + 2.182\phi, \quad (1)$$

where HJD is the Heliocentric Julian date of the observation and  $\phi$  is the rotational phase.

The SEMPOL spectropolarimeter involves a fibre feed from the Cassegrain focus of the AAT to UCLES, where the two polarisation states (in this case left- and right-hand circular polarisation) are outputted in two fibres to UCLES with both polarisation states being recorded simultaneously on the detector. The basic construction of the SEMPOL polarimeter consists of a quarter-wave plate (or quarter-wave Fresnel rhomb, depending on instrument setup) and a half-wave Fresnel rhomb. Spectropolarimetric observations in circularly polarised light (Stokes V) consist of a sequence of four exposures. Between the exposures the half-wave Fresnel rhomb is rotated between  $+45^\circ$  and  $-45^\circ$ . Thus the polarisation in each output fibre is alternated resulting in the removal of spurious polarisation signals from the telescope and polarimeter (at least to a first order approximation). Due to throughput losses in the spectropolarimeter setup the signal-to-noise (S/N) of spectropolarimetric data is usually lower than that obtained for straight spectroscopic observations. Further information on the operation of the SEMPOL spectropolarimeter can be found in Semel et al. (1993) and Donati et al. (1997, 2003).

As each Stokes V observation consists of 4 exposures this means that we generally have 4 times the number of Stokes I (intensity) observations as we do Stokes V. Note however that due to poor weather during some runs there are a few sequences on HD 141943 where we were only able to obtain a sequence of two exposures (see Table 1). The Stokes V profile can still be extracted from just two exposures, but with typically lower S/N.

The same detector and wavelength setup was used for all 4 observing runs. The detector was the EEV2 CCD with  $2048 \times 4096$   $13.5 \mu\text{m}$  square pixels. As the EEV2 is larger than the unvignetted field of UCLES a smaller window format ( $2048 \times 2746$  pixels) was used to reduce readout time. Using the 31 gr/mm grating, 46 orders (#129 to #84) were observed, giving a full wavelength coverage from  $\sim 4380 \text{ \AA}$  to  $\sim 6810 \text{ \AA}$ . For the May 2006 observations the chip was binned by 2 in the spectral direction and a 1 arcsec slit was used providing a resolution of  $\sim 50,000$  (i.e.  $\sim 6.0 \text{ km s}^{-1}$ ). For the spectropolarimetric observations (in 2007, 2009 and 2010) there was no binning and the fibre feed provided a resolution of  $\sim 70,000$  (i.e.  $\sim 4.3 \text{ km s}^{-1}$ ).

All raw frames were reduced into wavelength calibrated spectra using the ESPrIT (Echelle Spectra Reduction: an Interactive Tool) optimal extraction routines of Donati et al. (1997). As the Zeeman signatures in atomic lines are extremely small (typical relative amplitudes of 0.1 per cent or less) we have applied the technique of Least-Squares Deconvolution (LSD, Donati et al. 1997) to the over 2600 photospheric spectral lines in each echelle spectrum in order to create a single high S/N profile for each observation. The line mask used for the LSD was a G2 line list created from the Kurucz atomic database and ATLAS9 atmospheric models (Kurucz 1993).

The peak S/N of the initial Stokes I observations ranged from 30 to 260 (depending on observing conditions) while the peak S/N for the Stokes V observations (combining 2 or 4 exposures) was 50 to 330. LSD has been applied to both the Stokes I and Stokes V data resulting in S/N values of 540 to 930 for the Stokes I profiles and 1450 to 11600 for the Stokes V profiles. This corresponds to a multiplex gain of  $\sim 4 - 10$  for the Stokes I observations and  $\sim 35$  for the Stokes V observations. The multiplex gain for the Stokes I profiles is significantly less than that for the Stokes V profiles because, as pointed out by Donati et al. (1997), the technique of LSD appears to be not as suited to Stokes I as it is to Stokes V. In addition, the calculated S/N of the Stokes I LSD profiles are usually somewhat underestimated (see Section 4.1). Further information on LSD can be found in Donati et al. (1997) and Kochukhov, Makaganiuk & Piskunov (2010).

In order to correct for wavelength shifts of instrumental origin, each spectrum was shifted to match the Stokes I LSD profile of the telluric lines contained in the spectrum, as has been done by Donati et al. (2003) and other authors. This reduces the relative radial velocity shifts of the LSD profiles to  $\pm \sim 0.1 \text{ km s}^{-1}$ .

### 3 FUNDAMENTAL PARAMETERS OF HD 141943

In order to determine the surface topologies of HD 141943 the ZDI code needs to know several basic stellar parameters, namely the  $v \sin i$ , radial velocity, inclination of the rotation axis to the observer, and the temperature of the photosphere and spots on the stellar surface. The  $v \sin i$  and radial velocity are determined using the  $\chi^2$ -minimisation technique of Barnes et al. (2000). This is simply using those parameters that give the best fit to the dataset (lowest reduced  $\chi^2$  values).

According to Hillenbrand et al. (2008) HD 141943 is at a distance of 67 pc, has an effective temperature of 5805 K and a luminosity of  $2.7 L_\odot$ . Now these latter two values will be slightly higher for an unspotted star, but we do not know the spottedness of the star when the Hillenbrand et al. (2008) determinations were made. Given the level of spottedness shown on HD 141943 (see Section 4.1) we have assumed a spot coverage of 0% to 5% with the most likely coverage being 3%. This assumption, along with a spot-photosphere temperature difference of  $\sim 1900 \text{ K}$  (calculated from Fig. 7 of Berdyugina 2005), gives a photospheric temperature of  $\sim 5850 \text{ K}$ , a spot temperature of  $\sim 3950 \text{ K}$  and an unspotted luminosity of  $\sim 2.8 L_\odot$ .

As there are no error measurements given for the Hillenbrand et al. (2008) measurements we have assumed an error of  $\pm 100 \text{ K}$  in the photospheric temperature and  $\pm 0.1 L_\odot$  in the luminosity. These, along with the uncertain spot coverage at the time of the Hillenbrand et al. (2008) determinations and a  $v \sin i$  of  $35 \pm 0.5 \text{ km s}^{-1}$ , imply that HD 141943 has a radius of  $\sim 1.6 \pm 0.15 R_\odot$  and an inclination angle of  $\sim 70^\circ \pm 10^\circ$ . With a high inclination angle our imaging code (see Section 4) has difficulty determining if features are located in the Northern or Southern hemisphere so we have limited the inclination angle range to  $70^\circ \pm 10^\circ$ . Table 2 lists the basic stellar parameters of HD 141943 that we have determined for this study. As mentioned, there are no

**Table 1.** Logs of spectroscopic and spectropolarimetric AAT observations of HD 141943 for May 2006, March/April 2007, April 2009 and March/April 2010. The first two columns give the UT dates and times of the mid point of each observation, while the third column gives the exposure time. The fourth column gives the rotational phase of the observations calculated from equation 1. For the May 2006 observations the rotational phases have had 153.0 added to them, the March/April 2007 rotational phases have had 3.0 added to them, the April 2009 rotational phases have had 336.0 subtracted from them, while for the March/April 2010 observations the rotational phases have had 497.0 subtracted from them. This is so that all phases are shown as positive. The fifth column gives the signal-to-noise ratio of the resultant Stoves V LSD profile (only for the 2007, 2009 and 2010 spectropolarimetric data).

UT date	UT time	Exp. (sec.)	Rot. phase (+ 153.0)		UT date	UT time	Exp. (sec.)	Rot. phase (- 336.0)	S/N <sub>LSD</sub>
06 May 06	18:44:03 to 19:46:17	400, 300, 5×600	0.448 to 0.468		07 Apr 09	13:31:28 16:16:43	4×600 4×600	0.349 0.405	3827 3327
07 May 06	17:48:15 to 19:17:00	9×600	0.889 to 0.917			18:45:33	4×600	0.449	2251
08 May 06	17:16:24 to 19:27:28	13×600	1.337 to 1.379		08 Apr 09	13:25:37 18:51:41	4×600 4×800	0.805 0.909	5216 7225
09 May 06	17:26:23 to 19:38:43	13×600	1.798 to 1.840		09 Apr 09	13:59:27 17:07:59	4×800 4×800	1.274 1.334	5050 5760
10 May 06	16:53:01 to 19:30:00	15×600	2.246 to 2.296		10 Apr 09	14:33:60	2×800	1.744	5902
11 May 06	17:39:12 to 19:27:05	11×600	2.719 to 2.753		13 Apr 09	13:38:03	2×800	3.101	4730
UT date	UT time	Exp. (sec.)	Rot. phase (+ 3.0)	S/N <sub>LSD</sub>	UT date	UT time	Exp. (sec.)	Rot. phase (- 497.0)	S/N <sub>LSD</sub>
30 Mar 07	12:30:43	4×600	0.649	4948	25 Mar 10	13:50:14	4×800	0.674	10144
31 Mar 07	12:20:25	4×600	1.104	4507		18:57:49	4×800	0.772	6921
01 Apr 07	12:26:09	4×600	1.564	4656	26 Mar 10	14:08:19	4×800	1.138	9113
	18:40:53	4×600	1.684	4544		17:03:17	4×800	1.194	2034
02 Apr 07	12:23:33	4×600	2.022	5959		19:17:19	4×800	1.237	4127
	18:14:40	4×600	2.134	7715	27 Mar 10	14:57:05	4×800	1.612	8385
03 Apr 07	12:26:18	4×600	2.481	4606		16:49:52	2×800	1.648	4045
	18:56:19	4×600	2.605	5354		17:19:28	2×800	1.657	1470
04 Apr 07	13:07:40	4×600	2.953	5009		19:06:03	4×800	1.691	8869
	18:58:10	4×600	3.064	6980	28 Mar 10	14:33:02	4×800	2.063	8330
05 Apr 07	12:09:39	4×600	3.392	4873		17:05:00	4×800	2.111	5814
	15:42:02	4×600	3.460	4599	31 Mar 10	13:06:47	4×800	3.410	5950
	18:40:21	4×600	3.517	6617		19:01:29	4×800	3.523	9673
06 Apr 07	12:33:12	4×600	3.858	4915	01 Apr 10	13:30:07	4×800	3.876	7274
	16:18:35	4×600	3.930	6553		18:45:07	4×800	3.976	11575
	18:35:54	4×600	3.974	6700	02 Apr 10	13:03:07	4×800	4.326	9440
07 Apr 07	12:18:45	4×600	4.312	7035		18:45:48	4×800	4.435	8337
08 Apr 07	12:29:38	4×600	4.774	6963	03 Apr 10	13:16:00	4×800	4.788	8470
	16:11:27	4×600	4.844	6734		15:50:33	4×800	4.838	9398
	18:47:16	4×600	4.894	6847		18:55:30	4×800	4.896	4473
09 Apr 07	12:18:25	4×600	5.228	5992	04 Apr 10	14:22:06	4×800	5.268	7227
	16:11:12	4×600	5.303	7662		18:39:53	4×800	5.350	5186
	18:40:21	4×600	5.350	8100	05 Apr 10	12:05:53	4×800	5.683	4779
						13:05:15	4×800	5.702	5559

error measurements given for the Hillenbrand et al. (2008) measurements of effective temperature and luminosity, so the estimations of the errors in the stellar parameters of HD 141943 may well be underestimates.

From the values for photospheric temperature and unspotted luminosity we can determine the mass and age of HD 141943 from the evolutionary models of Siess, Dufour & Forestini (2000), see Fig. 1. This makes HD 141943 a  $\sim 1.3 M_{\odot}$  star of age  $\sim 17$  Myrs, in reasonable agreement with the values from Cutispoto et al. (2003), and thus it can be classified as a PMS star.

### 3.1 Is HD 141943 a binary?

Nordström et al. (2004) took 7 radial velocity measurements of HD 141943 over a 2979 day period (epochs and measurements were not given). Based on the fact that the standard error of each measurement was less than the standard deviation of the measurements they determined that HD 141943 only has a 31.4 per cent chance of having a constant radial velocity.

Our own radial velocity measurements also show some level of variation. Taking the radial velocity measurement of Waite et al. (2005) along with ours (Cutispoto et al. 1999 has some radial velocity measurements but the errors are too large to be useful) we have listed them in Table 3 to

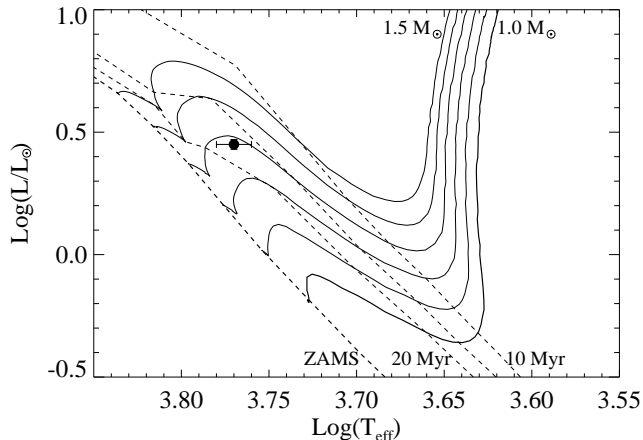


**Figure 1.** The evolutionary status of HD 141943 from the pre-main sequence models of Siess et al. (2000), using the 2007 updates. The solid lines are pre-main sequence evolutionary tracks for stellar masses of  $1.0 M_{\odot}$  to  $1.5 M_{\odot}$  in  $0.1 M_{\odot}$  steps, with the bold solid line denoting the  $1.0 M_{\odot}$  track. The dashed lines are age isochrones for stellar ages of 10 Myr, 15 Myr, 20 Myr, and the Zero-Age Main-Sequence (bold dashed line).

**Table 2.** Fundamental parameters of HD 141943 used/found in this study. The age and mass are from the theoretical isochrones of Siess et al. (2000) given in Fig. 1 and the equatorial rotation period has been determined from the differential rotation, see Paper II

Parameter	value
Age	$\sim 17$ Myrs
Mass	$\sim 1.3 M_{\odot}$
Photospheric temperature	$5850 \pm 100$ K <sup>a</sup>
Spot temperature	$\sim 3950$ K
Unspotted luminosity	$2.8 \pm 0.1 L_{\odot}^a$
Stellar radius	$1.6 \pm 0.15 R_{\odot}$
$v \sin i$	$35.0 \pm 0.5$ km s <sup>-1</sup>
Radial velocity ( $v_{\text{rad}}$ )	see Table 3
Inclination angle ( $i$ )	$70^{\circ} \pm 10^{\circ}$
Equatorial rotation period ( $P_{\text{eq}}$ )	$\sim 2.182$ days

<sup>a</sup>assumed error.

highlight the level of variation. The radial velocity for the 2006, 2007, 2009 and 2010 datasets has been calculated as part of the Doppler imaging process (see Section 4) and are for the entire dataset as a whole. Given that the radial velocity for 2007, 2009 and 2010 is constant (within error bars) it would mean that if HD 141943 is a binary then it would appear to have an elliptical orbit.

#### 4 IMAGES OF HD 141943

A surface image of a rapidly-rotating star can be generated through the inversion of a time series of Stokes I (brightness images) or Stokes V (magnetic images) profiles. The brightness and magnetic topologies of HD 141943 were created using the ZDI code of Brown et al. (1991) and Donati & Brown (1997) using a linear limb-darkening coefficient of 0.66. As the inversion is an ill-posed problem, an infinite number of solutions can be found that fit the data to

**Table 3.** Log of radial velocity measurements of HD 141943 from these observations plus that of Waite et al. (2005). For the 2006, 2007, 2009 and 2010 datasets the HJD given is for the mid-point of the observations. The errors in the radial velocity measures represent a  $3\sigma$  change in the reduced  $\chi^2$  values (see text).

Data set	HJD (2450000.0+)	Radial Velocity (km s <sup>-1</sup> )
2005	2396.828	$-1.5 \pm 1.0$
2006	3864.801	$-0.6 \pm 0.1$
2007	4195.154	$0.1 \pm 0.1$
2009	4932.071	$0.1 \pm 0.1$
2010	5286.564	$0.2 \pm 0.1$

the noise level. Therefore a regularisation scheme is usually introduced to determine a unique solution with the role of the regularisation scheme being reduced with high quality data. Our imaging code uses the Skilling & Bryan (1984) maximum-entropy regularisation scheme. This scheme has the effect of producing images with the minimum amount of information required to fit the data to the noise level.

#### 4.1 Brightness images

The imaging code to reconstruct the spot features on HD 141943 uses a two-temperature model (one for the spots and the other for the unspotted photosphere) as described by Collier Cameron (1992). Each pixel on the stellar surface is reconstructed for spot occupancy (the local relative area occupied by cool spots) and varies from 0 (no spots) to 1 (maximum spottedness). Following on from Unruh & Collier Cameron (1995), who showed that there is little change in spot topology when using a synthetic profile over profiles created from slowly rotating comparison stars, we have used Gaussian profiles to represent the profiles of both the spots and the photosphere. This is almost standard practice now with a number of previous works doing the same (i.e. Petit et al. 2004b; Marsden et al. 2005b, 2006a; Jeffers & Donati 2008). As has done for the two previous young early-G stars for which spot topologies have been obtained by this method (R58, Marsden et al. 2005b and HD 171488, Marsden et al. 2006a) we have used the same Gaussian to represent both the spot and photosphere. The full-width at half-maximum (FWHM) of the Gaussians used were slightly different for the spectroscopic and spectropolarimetric data sets, with a FWHM of  $10$  km s<sup>-1</sup> used for the spectroscopic data set and a FWHM of  $9$  km s<sup>-1</sup> used for the spectropolarimetric data sets. These FWHM were determined from matching the FWHM of the Moon's LSD profile taken with the same instrumental setup during each observing run.

The maximum-entropy brightness images for HD 141943 for the 4 observing epochs are shown in Fig. 2 (2006 observations), the top-left image of Fig. 3 (2007 observations), the top-left image of Fig. 4 (2009 observations) and the top-left image of Fig 5 (2010 observations). These images were created fitting the data down to reduced  $\chi^2$  values of 0.2, 0.3, 0.4 and 0.3 for the 2006, 2007, 2009 and 2010 datasets respectively. As explained in Petit et al. (2004b) a reduced  $\chi^2$  value smaller than unity can be achieved because, as mentioned in Section 2, the S/N calculated for the

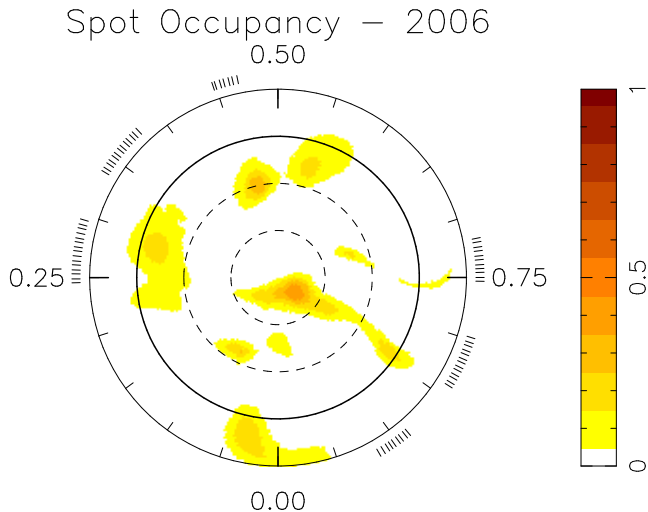


**Figure 2.** Maximum entropy brightness image reconstruction for HD 141943, May 2006. The image is a flattened polar projection looking down on the north pole and extending down to  $-30^\circ$  latitude. The bold line denotes the equator and the dashed lines are  $+30^\circ$  and  $+60^\circ$  latitude parallels. The radial ticks outside the plot indicate the phases at which the star was observed. The image has a spot filling factor of 0.021 (or 2.1 per cent). The image incorporates the measured surface differential rotation, see Paper II.

Stokes I LSD profiles are underestimated. This has no effect on the maps produced. Fits of the modelled profiles to the observed LSD profiles are given in Fig. 6 (2006 observations), Fig. 7 (2007 observations), Fig. 8 (2009 observations) and Fig 9 (2010 observations). The epochs of the observations, as calculated from the midpoint of each dataset, are: 2006.352, 2007.257, 2009.273 and 2010.244 in decimal years.

The brightness images of HD 141943 show that at all 4 epochs HD 141943 had a smallish polar spot and numerous low-latitude features situated mostly between the equator and  $\sim +30^\circ$  latitude. In the May 2006 image (Fig. 2) there appears to be some features below the equator and above  $+30^\circ$ . However, as there are no observations around these phases it could well be that the code has had trouble determining the latitude of spot features that are only seen in the wings of the profiles.

The spot filling factor (the level of spot coverage over the entire stellar surface) is also very similar over the 4 epochs. In 2006 the spot coverage was 2.1 per cent, in 2007 it was 3.1 per cent, in 2009 2.7 per cent and in 2010 it was 2.9 per cent. The reason for the slightly lower value of spot coverage for the 2006 dataset may well be due to the limited phase coverage of the observations, see Fig. 2. Thus some spots in these observing gaps may not have been recovered.

The variation in spot occupancy with stellar latitude is given in Fig. 10, which plots fractional spottedness versus stellar latitude. Fractional spottedness is defined as:

$$F(\theta) = \frac{S(\theta)\cos(\theta)d\theta}{2} \quad (2)$$

where,  $S(\theta)$  is the average spot occupancy at latitude  $\theta$  and  $d\theta$  is the latitude width of each latitude ring.

It has been reported that active solar-type stars show evidence of active longitudes, where certain longitudes (usually two longitudes around  $180^\circ$  apart) are more active than

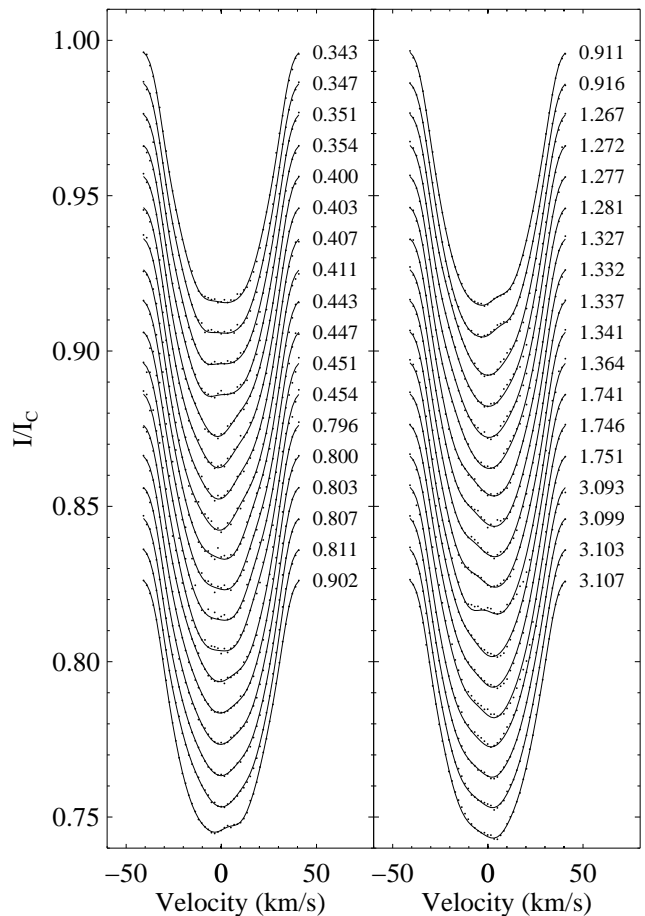


**Figure 8.** Maximum entropy fits for the Stokes I LSD profiles of HD 141943, April 2009. As described in Fig. 6, the dots represent the observed LSD profiles while the lines represent the fits to the profiles produced by the imaging code.

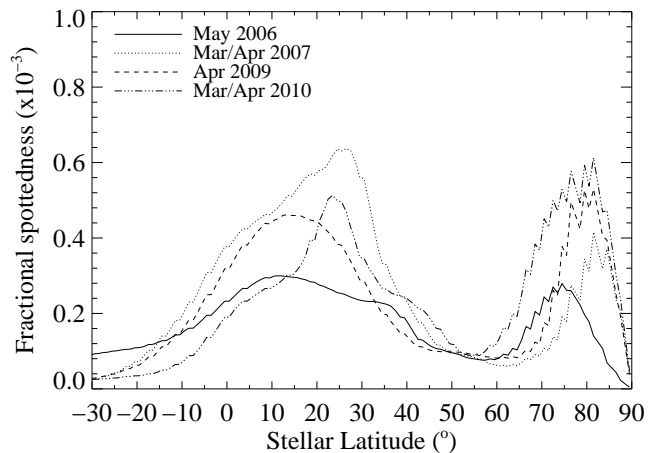


**Figure 10.** Fractional spottedness versus stellar latitude for HD141943. Fractional spottedness is based on the average spot occupancy at each latitude and is defined by equation 2.

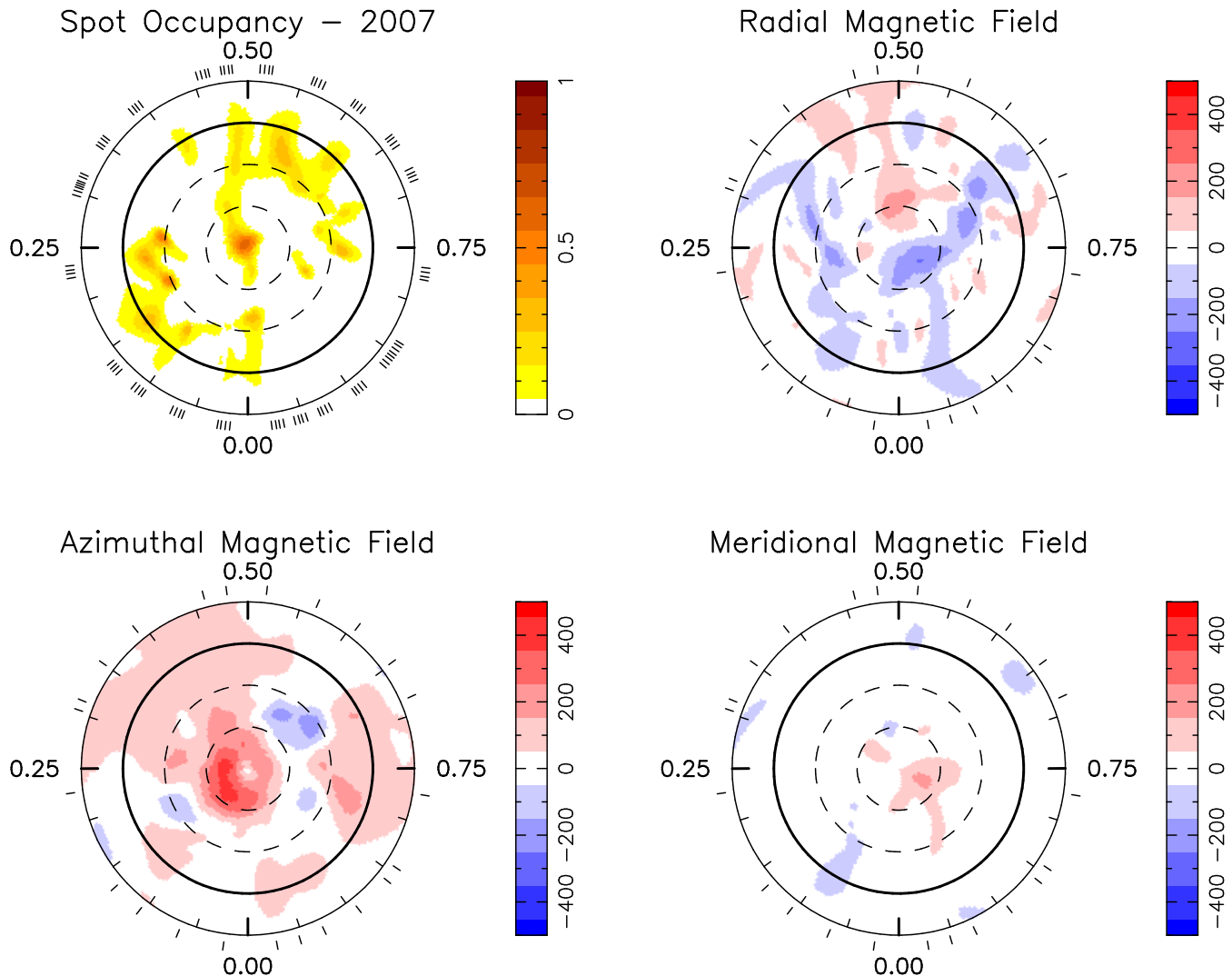


**Figure 3.** Maximum entropy brightness and magnetic image reconstructions for HD 141943, March/April 2007. The images are flattened polar projections as described in Fig. 2. The scale in the magnetic images is in Gauss. The brightness image (top-left) has a spot filling factor of 0.031 (or 3.1 per cent), while the magnetic images have a mean field modulus of 91.3 G. The images have been created with the inclusion of the surface differential rotation of the star, see Paper II.

others on the stellar surface (i.e. Berdyugina & Tuominen 1998; Järvinen et al. 2005). In order to test this we have plotted the average spottedness versus stellar rotational phase for all 4 epochs of HD 141943 observations. This is displayed in Fig. 11. In case the polar spot is affecting the results we have plotted the average spottedness for both (a)  $0^\circ$  to  $+90^\circ$  and (b)  $0^\circ$  to  $+60^\circ$  in latitude.

For the 2006 and 2009 datasets there is very little evidence for active longitudes on the stellar surface and the limited phases observed in these datasets may well be influencing this result. For the well sampled 2007 dataset, and looking at the top-left image in Fig. 3, there appears to be a slight enhancement of the lower-latitude spots around phases  $\sim 0.25$  and  $\sim 0.55$ . However as shown in Fig. 11(b) these enhancements are rather broad. For the 2010 dataset there appears to be an increase in the spot coverage at phase  $\sim 0.00$ . However, this is reduced when only considering low-latitude features (Fig. 11(b)) and when looking at the top-left image in Fig. 5 the enhancement could be caused by the

extension of the polar spot to slightly lower-latitudes around phase  $\sim 0.00$  in the 2010 epoch. There would not appear to be any evidence of another active longitude on the star in 2010. We do not feel that these represent strong evidence for active longitudes on HD 141943.

#### 4.2 Magnetic images

The magnetic field topology for HD 141943 has been reconstructed for three epochs using the modelling of Donati & Brown (1997) and including the spherical harmonic expansion of the surface magnetic field by Donati et al. (2006). The magnetic reconstruction is done assuming a generalised potential field plus a toroidal field using a high order ( $l \leq 30$ ) spherical harmonic expansion. A limit of  $l_{\max} = 30$  was chosen for the spherical harmonic expansion, as beyond this limit the magnetic topologies remain essentially unchanged.

Various weighting schemes can be applied to the spher-

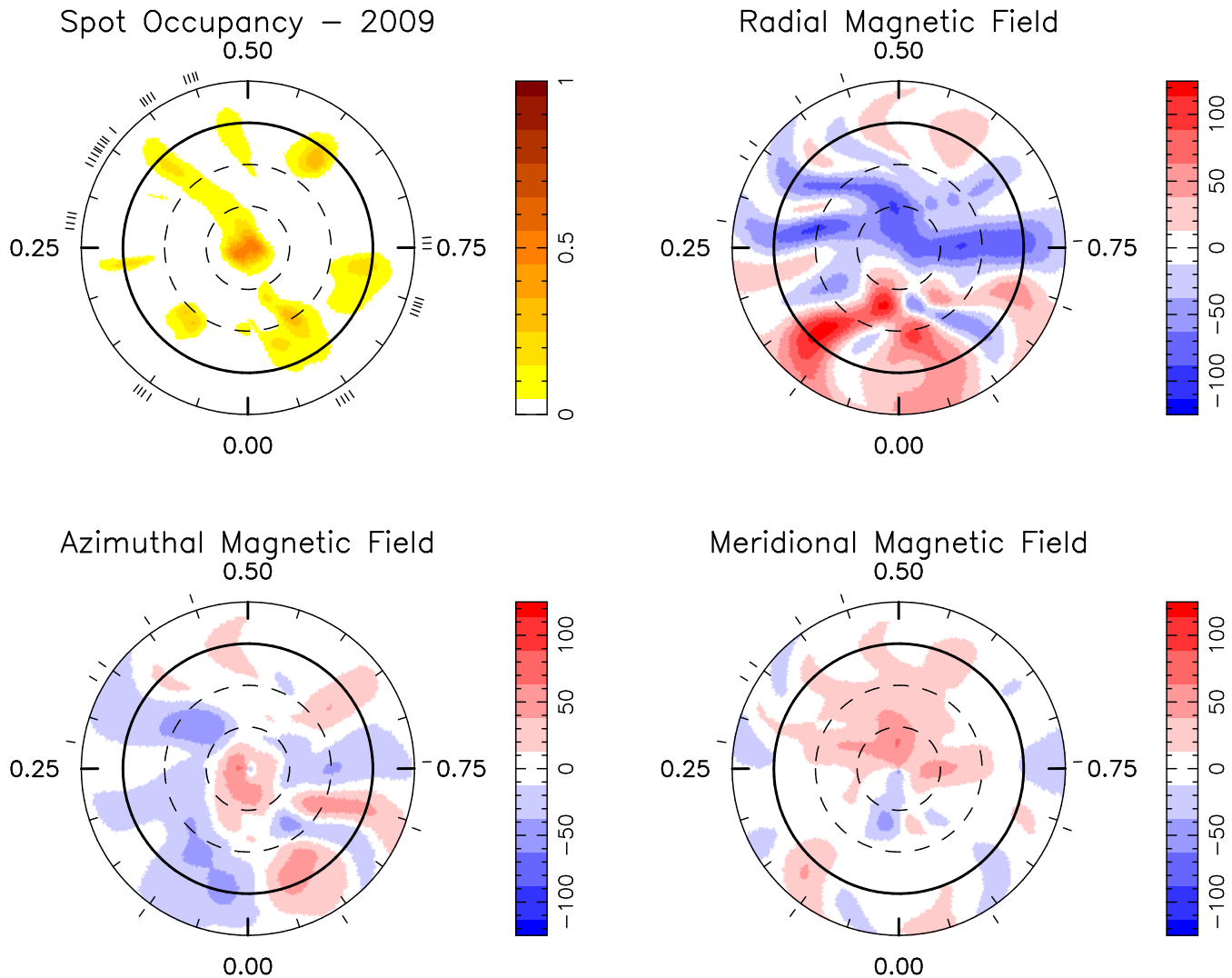


**Figure 4.** Maximum entropy brightness and magnetic image reconstructions for HD 141943, April 2009. The images are flattened polar projections as described in Fig. 2. The brightness image (top-left) has a spot filling factor of 0.027 (or 2.7 per cent), while the magnetic images have a mean field modulus of 36.6 G. The images incorporate the measured surface differential rotation, see Paper II. Note the different scale in the magnetic images compared to Fig. 3.

ical harmonic expansion so that the reconstruction favours different magnetic field topologies. Following the principle of Occam’s razor, we have used a weighting scheme that favours “simpler” magnetic fields (i.e. those with lower  $l$  values) while still reconstructing a similar overall magnetic topology to an unweighted reconstruction. Details of the spherical harmonic technique can be found in Donati et al. (2006).

It should be noted that the April 2009 dataset can be modelled using a purely potential field without the need to include a toroidal field, but this may be due to the limited data in the 2009 observations. The March/April 2007 and March/April 2010 datasets however, cannot be modelled to a reduced  $\chi^2$  value of 1.0 without the inclusion of a toroidal field component. Thus we have assumed a potential field plus toroidal field when modelling all three datasets.

Using the Stokes V LSD profiles the magnetic imaging code reconstructs images of radial, azimuthal and meridional field on the stellar surface, assuming a weak magnetic

field and a constant Gaussian profile over the stellar surface (see Donati et al. 2003). Radial field is defined as field in/out of the stellar surface, with positive field being field lines directed outward from the surface. Azimuthal field is defined as field wrapped around the rotational axis of the star, with positive being defined as counterclockwise. Meridional field is defined as field following lines of longitude north and south, with positive being northward.

The reconstructed magnetic topologies from the March/April 2007, April 2009 and March/April 2010 epochs are given in Fig. 3, Fig. 4 and Fig. 5 respectively. The fits to the observed Stokes V LSD profiles are given in Fig. 12 (2007 observations), Fig. 13 (2009 observations) and Fig. 14 (2010 observations). All three epochs were fitted to a reduced  $\chi^2$  value of 1.0. Table 4 list the magnetic quantities derived from the magnetic maps in Fig. 3, Fig. 4 and Fig. 5 and Fig. 15 plots these values out. As done in Petit et al. (2008) we have varied the input parameters (namely inclination angle,  $v \sin i$ , rotational period and differential rotation)



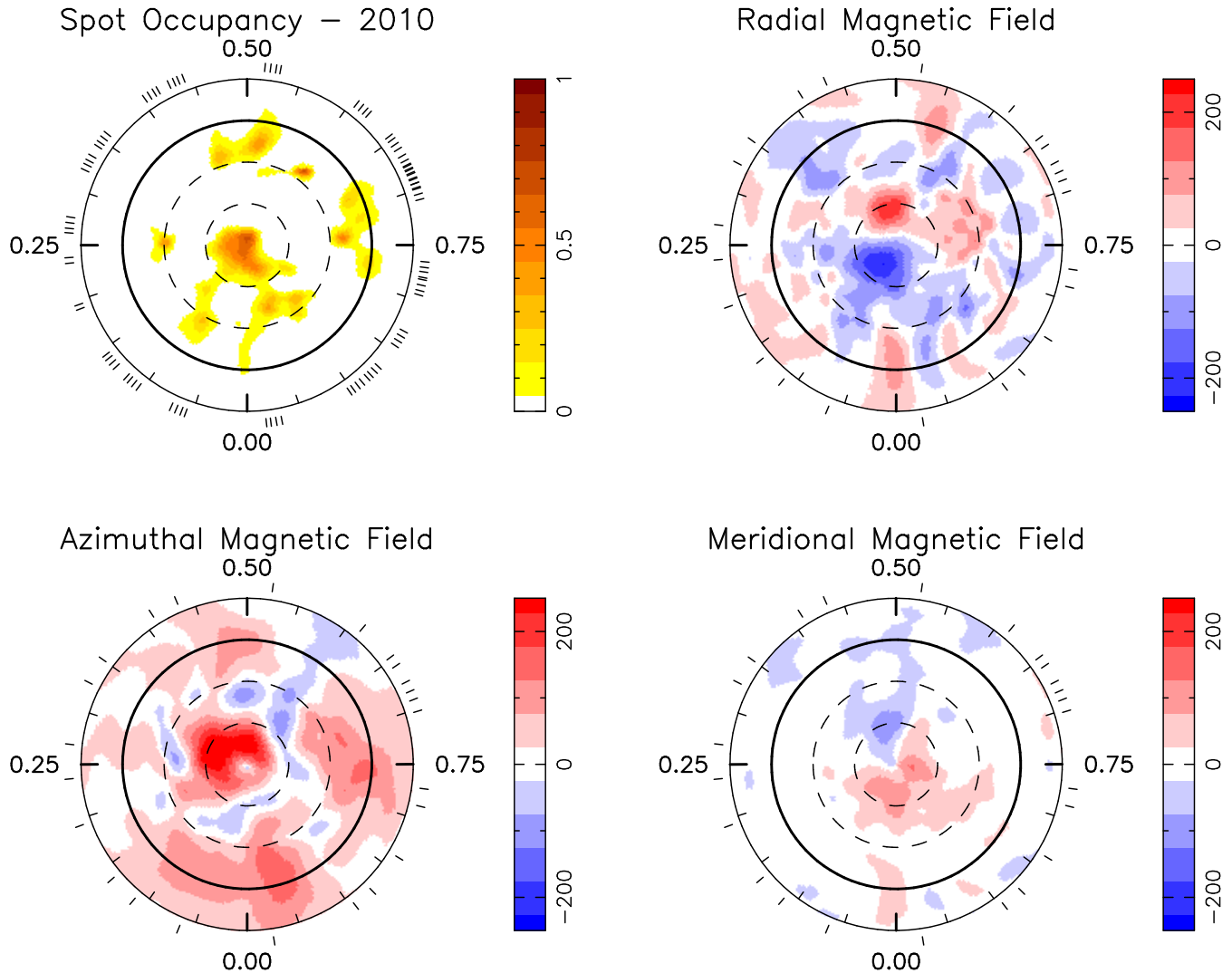


**Figure 5.** Maximum entropy brightness and magnetic image reconstructions for HD 141943, March/April 2010. The images are flattened polar projections as described in Fig. 2. The brightness image (top-left) has a spot filling factor of 0.029 (or 2.9 per cent), while the magnetic images have a mean field modulus of 70.9 G. The images incorporate the measured surface differential rotation, see Paper II. Note the different scale in the magnetic images compared to Fig. 3 and Fig 4.

by the errors given in Table 2 and Paper II to determine the possible errors in the magnetic quantities given in Table 4. These errors apply only for the simplified weighting scheme we have used in our reconstructions (see above) and assuming a potential plus toroidal field in the magnetic field reconstruction. They are thus likely to be lower-limits.

The reconstructed magnetic topology maps shown in Fig. 3, Fig. 4 and Fig. 5 show the maximum entropy reconstruction of the large-scale magnetic topology of HD 141943 at the three epochs, 2007.257, 2009.273 and 2010.244. The magnetic imaging code mainly reconstructs the large-scale magnetic topology on the stellar surface of the star, as magnetic flux that is contained in small dipoles below the resolution limit of the observations ( $\sim 11^\circ$  in longitude at the stellar equator) is likely to cancel out and not be recovered.

As has been previously described (i.e. Donati & Brown 1997) the technique of ZDI sometimes suffers cross-talk between radial and meridional components of the magnetic field for low-latitude features. However, this effect is mainly

present in stars with low inclination angles. Given the relatively large inclination angle of HD 141943 ( $i \sim 70^\circ$ ) this effect should be minimal. Conversely the sensitivity of ZDI to low-latitude meridional fields decreases significantly with an increase in stellar inclination, and thus the meridional field topologies of HD 141943 (lower-right images of Fig. 3, Fig. 4 and Fig. 5) may well miss some meridional field that has not been reconstructed. However, given the lack of meridional field seen on most active stars we believe that if there is any missing field it should be minimal.

In the April 2009 observations, there is a large gap in the observations between a phase of  $\sim 0.45$  to  $\sim 0.75$ . This is most likely to have an effect on the recovered radial magnetic field (as ZDI is mostly sensitive to radial field around the phase of the observation and to azimuthal field around 0.2 phase from the observation). This could explain the slightly lower intensity of the radial magnetic features (top-right image of Fig. 4) at these phases and may well mean that the

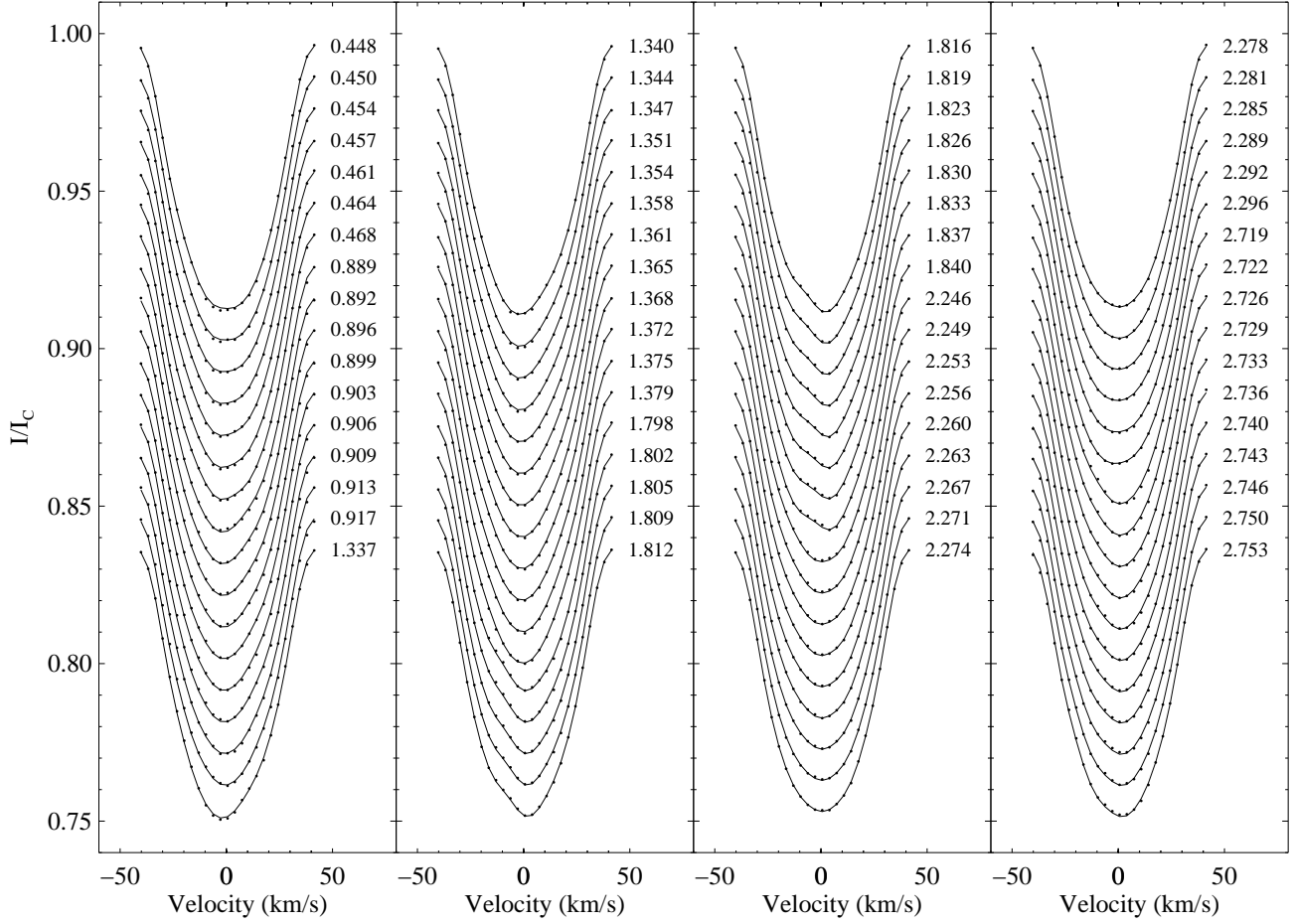


**Figure 6.** Maximum entropy fits for the Stokes I LSD profiles of HD 141943, May 2006. The dots represent the observed LSD profiles while the lines represent the fits to the profiles produced by the imaging code. Each profile is shifted down by 0.01 for graphical purposes. The rotational phases at which the observations took place are indicated to the right of each profile.

**Table 4.** Magnetic quantities derived from the magnetic maps in Fig. 3, Fig. 4 and Fig. 5. The first column is the epoch of the observation, while the second column is the mean field modulus over the stellar surface. The third and fourth columns are the per cent of the large scale magnetic energy in the reconstructed poloidal and toroidal field components. The fifth, sixth and seventh columns are the per cent of the poloidal magnetic energy in dipole ( $l = 1$ ), quadrupole ( $l = 2$ ) and octupole components ( $l = 3$ ), while the eighth, ninth and tenth columns are the same for the toroidal field. Columns 11 and 12 are the per cent of the poloidal and toroidal field that are axisymmetric ( $m = 0$ ).

Epoch	$\langle B_{\text{mod}} \rangle$	% pol. en.	% tor. en.	% pol. dip.	% pol. quad.	% pol. oct.	% tor. dip.	% tor. quad.	% tor. oct.	% axis sym. pol.	% axis sym. tor.
2007.257	$91^{+26}_{-11}$ G	$47^{+8}_{-9}$	$52^{+9}_{-7}$	$16^{+1}_{-5}$	$10^{+4}_{-3}$	$15^{+2}_{-4}$	$32^{+9}_{-9}$	$4^{+4}_{-3}$	$4^{+8}_{-3}$	$28^{+2}_{-5}$	$73^{+7}_{-2}$
2009.273	$37^{+4}_{-4}$ G	$82^{+2}_{-2}$	$17^{+3}_{-1}$	$29^{+2}_{-9}$	$20^{+5}_{-6}$	$6^{+3}_{-2}$	$7^{+4}_{-4}$	$24^{+8}_{-6}$	$12^{+3}_{-4}$	$22^{+10}_{-9}$	$74^{+5}_{-5}$
2010.244	$71^{+19}_{-10}$ G	$50^{+3}_{-5}$	$50^{+5}_{-3}$	$6^{+3}_{-2}$	$9^{+1}_{-2}$	$21^{+7}_{-6}$	$37^{+5}_{-11}$	$9^{+2}_{-3}$	$2^{+4}_{-0}$	$30^{+7}_{-10}$	$71^{+6}_{-1}$

per cent of poloidal magnetic energy in Table 4 is slightly underestimated for the April 2009 observations.

The first thing to notice from Table 4 is that the mean magnetic field of the 2007 and 2010 maps is significantly higher than that of the 2009 maps ( $\sim 91$  G and  $\sim 71$  G compared to  $\sim 37$  G). This could either be a significant change in the magnetic field strength on HD 141943 during 2009 or it may well be due to the limited amount (and poorer quality) of observations in the 2009 dataset compared with

that of 2007 and 2010. To test this we took only a limited number of profiles from the 2007 and 2010 datasets that had a similar phase coverage to that of the 2009 dataset. This had the result of decreasing the mean magnetic field to  $\sim 66$  G and  $\sim 51$  G for the 2007 and 2010 datasets respectively. In addition, we artificially increased the S/N of the Apr 2009 profiles by fitting the data to a reduced  $\chi^2$  of 0.8, which had the effect of almost doubling the mean magnetic field on the star to  $\sim 60$  G. Thus we believe that the poor quality of

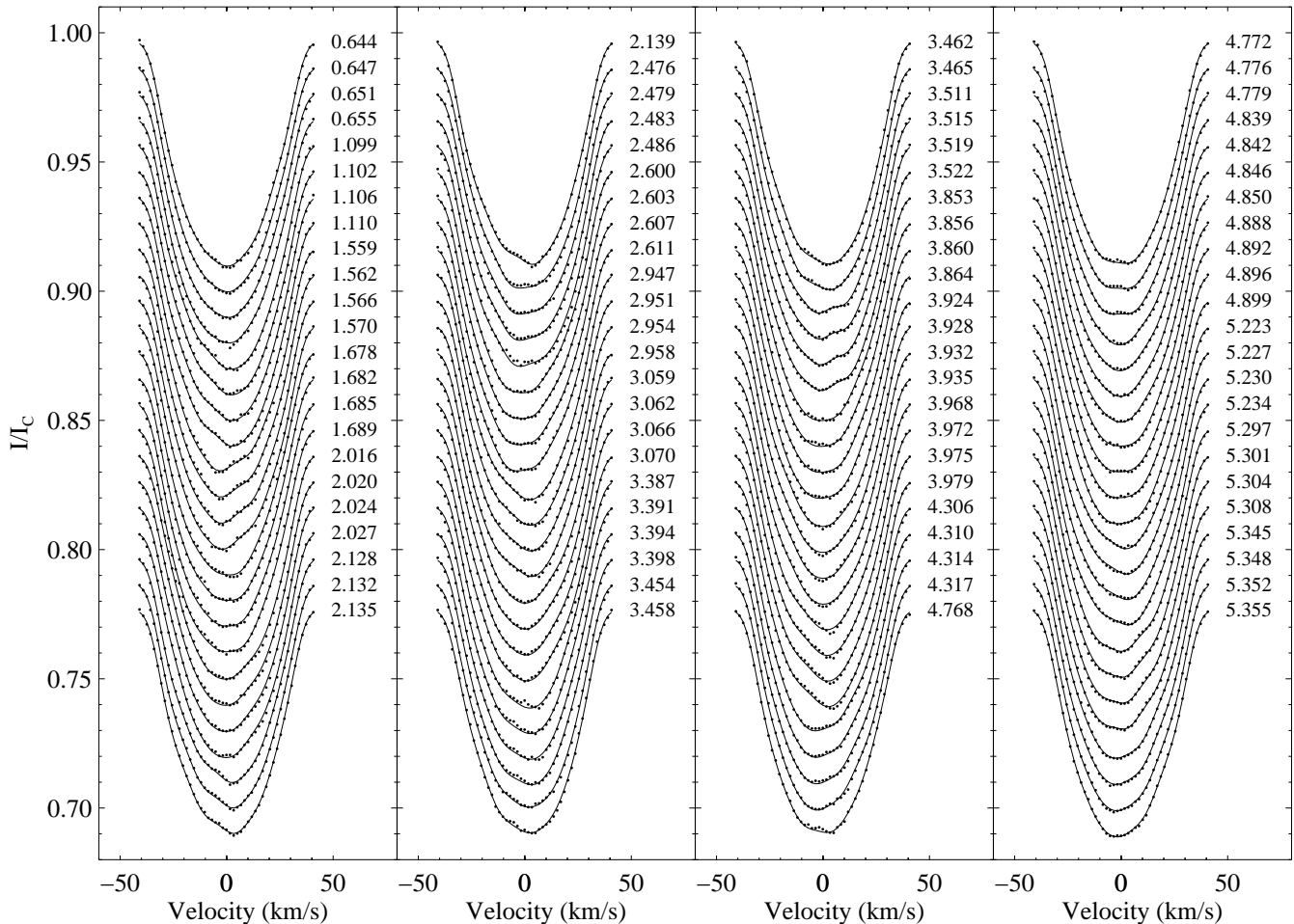


**Figure 7.** Maximum entropy fits for the Stokes I LSD profiles of HD 141943, March/April 2007. Again the dots represent the observed LSD profiles while the lines represent the fits to the profiles produced by the imaging code as described in Fig. 6.

the April 2009 data could well be the reason for the change in mean magnetic field on the star, rather than any actual change in the magnetic field strength of the star.

The other obvious feature of Table 4 is the observation that the balance between poloidal and toroidal magnetic energy changed dramatically in 2009 compared to the 2007 and 2010 epochs, being roughly balanced in 2007 and 2010 but being dominated by the poloidal component in 2009. Using the magnetic maps created from a limited number of profiles in 2007 and 2010 (see above) we tested to see if the limited dataset in April 2009 could have affected the ratio of poloidal and toroidal magnetic energy seen in the 2009 observations. Reducing the number of profiles used in the creation of the magnetic map had very little effect on the balance between poloidal and toroidal field in both the 2007 and 2010 datasets (still almost evenly balanced). Thus we believe that the change in the ratio of poloidal and toroidal magnetic energy in the 2009 epoch may well be real, but we cannot rule out the poor dataset in 2009 being responsible.

The major effect that limiting the number of observations in the 2007 and 2010 datasets had was to slightly decrease the complexity of the magnetic field (with more energy in octupole components or lower) and this may explain

the slight lowering of the complexity of the poloidal field seen in the 2009 dataset.

As was done for the spot features, the variation in magnetic field with stellar latitude is given in Fig. 16. This is again determined using equation 2, but with  $S(\theta)$  representing the value of the magnetic field at each latitude rather than spot occupancy. We have also determined the variation in magnetic field with longitude, averaging the absolute value of the magnetic field at each longitude. This is shown in Fig. 17.

Fig. 16 shows that the radial magnetic field of HD 141943 is predominantly negative at all epochs for latitudes above  $\sim 0^\circ$ . The azimuthal field is predominantly positive at all latitudes in 2007 and 2010 but in 2009 it is positive at high latitudes and predominantly negative at latitudes below  $\sim 60^\circ$ . Although we feel that this change in the azimuthal field, along with the change in the ratio of poloidal/toroidal field, is possible evidence for a changing magnetic field on HD 141943, we cannot rule out the poor 2009 dataset being responsible. As with the brightness images, Fig. 17 shows little or no evidence of active longitudes in the magnetic fields on HD 141943.

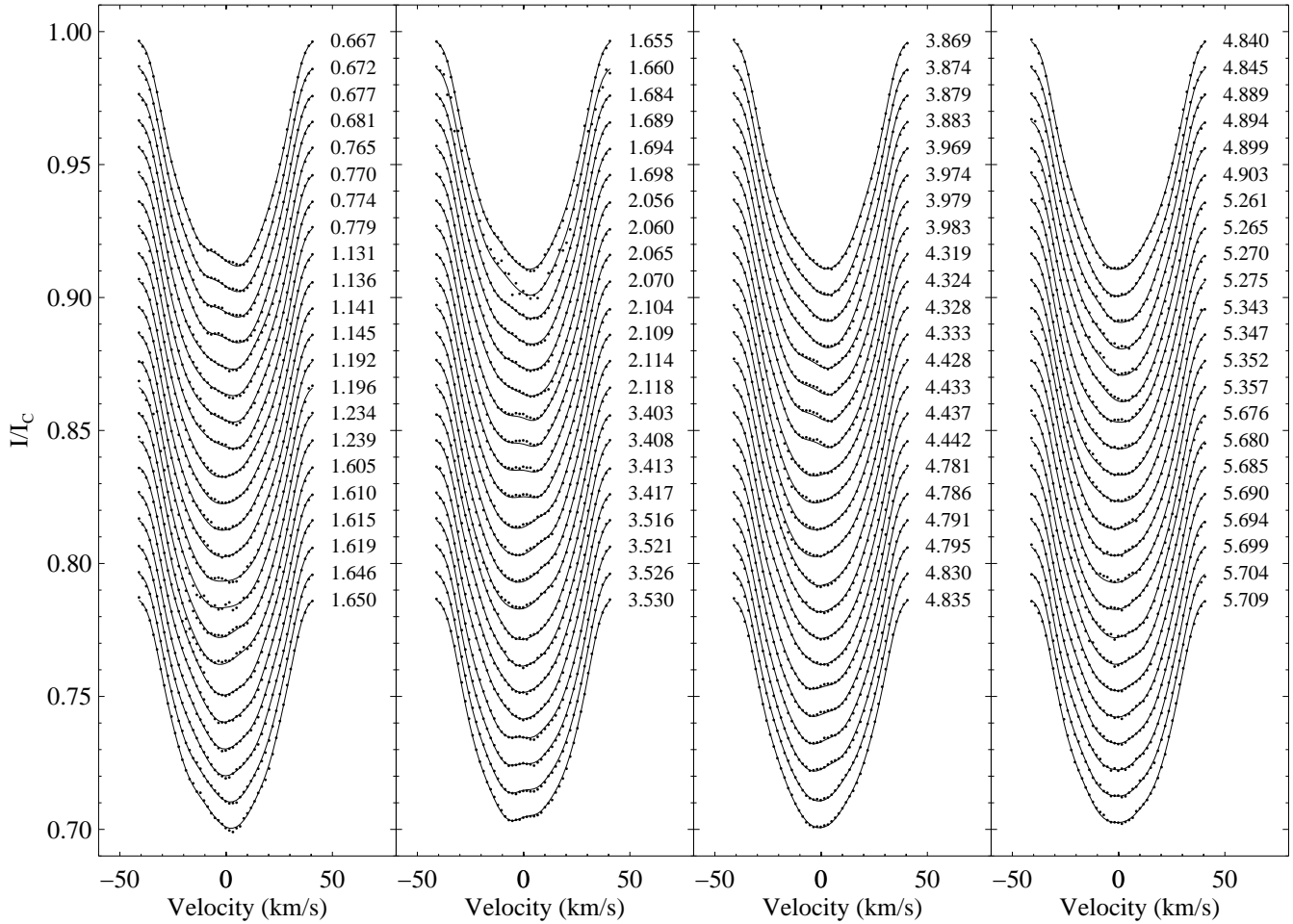


**Figure 9.** Maximum entropy fits for the Stokes I LSD profiles of HD 141943, March/April 2010. As described in Fig. 6, the dots represent the observed LSD profiles while the lines represent the fits to the profiles produced by the imaging code.

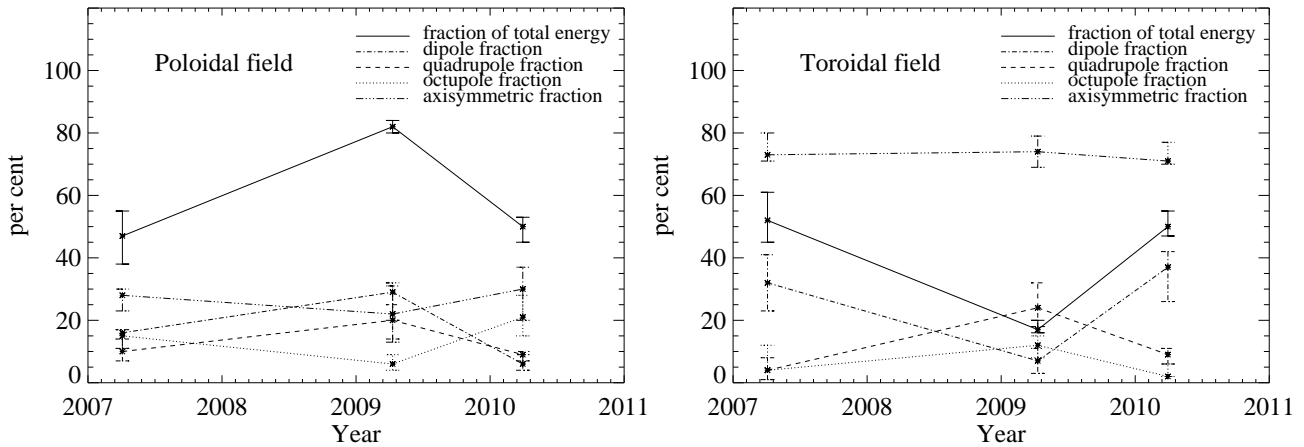


**Figure 15.** Plot of the magnetic parameters of HD 141943 given in Table 4 for the poloidal field (right-hand plot) and toroidal field (left-hand plot). The solid line is the per cent of the large scale energy in the reconstructed poloidal or toroidal field components, the percent of the poloidal or toroidal magnetic energy in dipole (dot-dashed line), quadrupole (dashed line) and octupole (dotted line) components are also given. The percent of the poloidal or toroidal field that is axisymmetric is plotted as a triple-dot-dashed line.

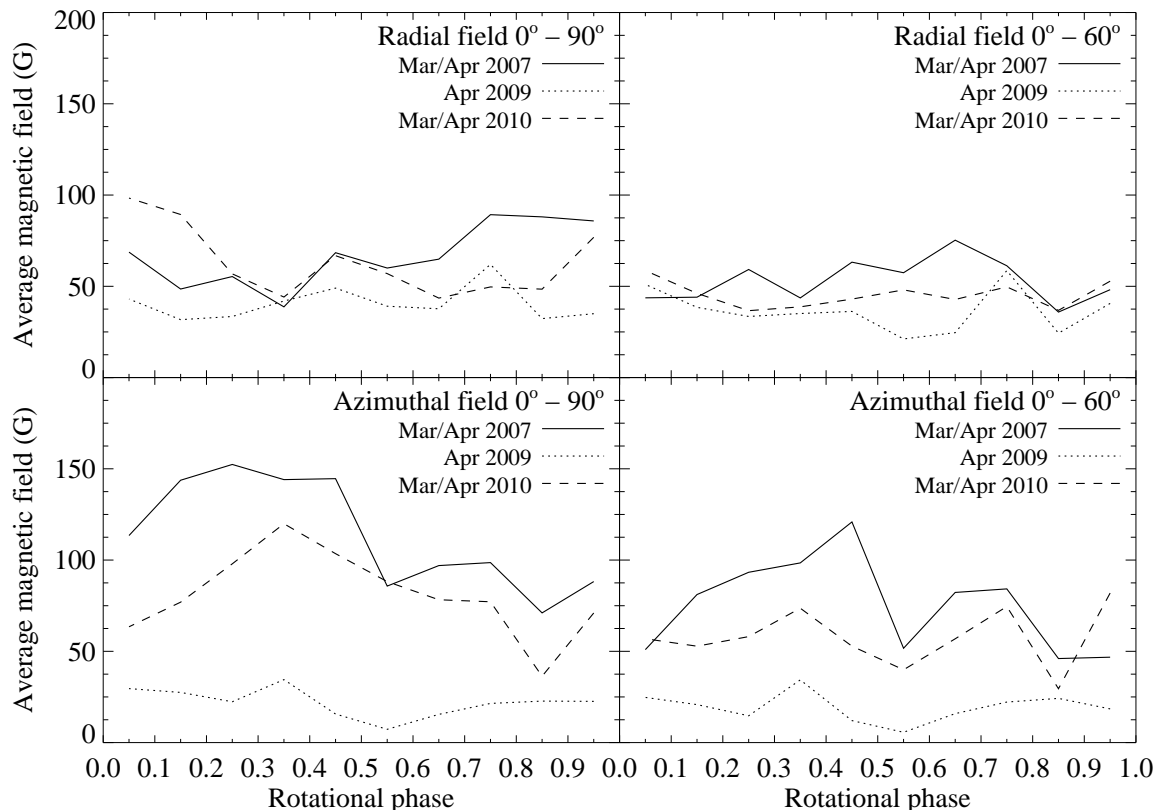


**Figure 17.** Average of the absolute value of the radial magnetic field (upper plots) and the azimuthal magnetic field (lower plots) versus stellar rotational phase for HD141943, averaged over  $0^\circ$  to  $+90^\circ$  (left-hand plots) and  $0^\circ$  to  $+60^\circ$  (right-hand plots) latitude. As was done in Fig. 11, the phase has been binned into 0.1 steps to remove any small scale variations.

## 5 DISCUSSION

HD 141943 is only the second (or third including the results for HD 106506 by Waite et al. 2010) young early-G star for which the large-scale magnetic topology has been determined, the other being HD 171488 (Marsden et al. 2006a; Jeffers & Donati 2008; Jeffers et al. 2010). However, there have been five young early-G stars for which spot maps and differential rotation measures have been determined (and a number of others that have just spot maps, see Table 4 in Strassmeier et al. 2003). Along with HD 141943, HD 171488 and HD 106506, the other two stars are, R58 (Marsden et al. 2005a,b) and LQ Lup (Donati et al. 2000). For comparative purposes in this discussion the stellar parameters of all these five stars are given in Table 5.

### 5.1 Spot topology

The surface spot topology of HD 141943 at four epochs is shown in Fig. 2, Fig. 3 (top-left image), Fig. 4 (top-left image) and Fig. 5 (top-left image). The 4 maps show that the spot topology of HD 141943 was remarkably consistent over the span of the observations ( $\sim 4$  years). All maps show that HD 141943 has a smallish polar spot with a number of lower-latitude features situated predominantly between the equator and  $+30^\circ$  latitude, with only the 2010 epoch showing some significant spot features between  $+30^\circ$  and  $+60^\circ$  latitude at around phase  $\sim 0.90$ . The total spot coverage for all

4 epochs is also very similar ranging from 2.1 per cent to 3.1 per cent.

Comparing these maps to those of other young early-G stars created using the same imaging code, such as R58 (Marsden et al. 2005b), LQ Lup (Donati et al. 2000), HD 171488 (Marsden et al. 2006a; Jeffers & Donati 2008; Jeffers et al. 2010) and HD 106506 (Waite et al. 2010), it is quite noticeable that while all stars appear to have some lower-latitude features, the polar spot on HD 141943 is significantly smaller than that shown by these other targets. Marsden et al. (2005b) has shown that starspot mapping assuming high stellar inclination angles leads to a dramatic increase in the amount of polar spot features needed to match the observed deviations in the LSD profiles. Given that HD 141943 has a higher stellar inclination than the other stars listed in Table 5 it is not an incorrectly determined stellar inclination that is responsible for the small polar spot on HD 141943.

As can be seen in Table 5, HD 141943 is the second youngest and second most massive (behind HD 106506) of the young early-G stars so far imaged using this code. It also has the shallowest convective zone (as a function of the stellar radius) and is the slowest rotator of the five. Which of these factors is responsible for the small polar spot seen on HD 141943 is still open for debate. The young early-K star LQ Hya has a rotation rate somewhere between that of HD 141943 and HD 171488 ( $P \sim 1.6$  d) and has a convective zone depth of  $\sim 0.29 R_*$ . In some spot maps LQ Hya also show a smallish polar spot (Donati et al. 2003), although the maps

**Table 5.** Comparison of the stellar parameters of the five young early-G stars that have had their spot topology and surface differential rotation measured using Doppler imaging. The first three, HD 141943, HD 106506 and HD 171488, have also had their magnetic topologies imaged. Except where noted, the data for HD 141943 are taken from this paper and Paper II, the data for HD 106506 are from Waite et al. (2010) and that for HD 171488 are from Strassmeier et al. (2003) and Marsden et al. (2006a). The data for R58 comes from Marsden et al. (2005b) and the data for LQ Lup from Donati et al. (2000). The values for the depth of the convective zone are from Siess et al. (2000).

Parameter	HD 141943	HD 106506	HD 171488	R58	LQ Lup
(B-V)	0.65 <sup>a</sup>	0.605	0.62 <sup>a</sup>	0.61 <sup>b</sup>	0.69 <sup>c</sup>
Age (Myrs)	~17	≲10	30 – 50	35 ± 5	25 ± 10
Mass (M <sub>⊙</sub> )	~1.3	1.5 ± 0.1	1.20 ± 0.02	1.15 ± 0.05	1.16 ± 0.04
Radius (R <sub>⊙</sub> )	1.6 ± 0.1	2.15 ± 0.26	1.15 ± 0.08	1.18 <sup>+0.17</sup> <sub>-0.10</sub>	1.22 ± 0.12
Inclination (°)	70 ± 10	65 ± 5	60 ± 10	60 ± 10	35 ± 5
Convective zone (R <sub>*</sub> )	~0.16 [0.26 R <sub>⊙</sub> ]	~0.22 [0.47 R <sub>⊙</sub> ]	~0.21 [0.24 R <sub>⊙</sub> ]	~0.21 [0.25 R <sub>⊙</sub> ]	~0.26 [0.32 R <sub>⊙</sub> ]
Equatorial rotation period (d)	~2.2	~1.4	~1.3	~0.56	~0.31

<sup>a</sup>from Cutispoto et al. (2002); <sup>b</sup>from Randich (2001), dereddened value; <sup>c</sup>from Wichmann et al. (1997).

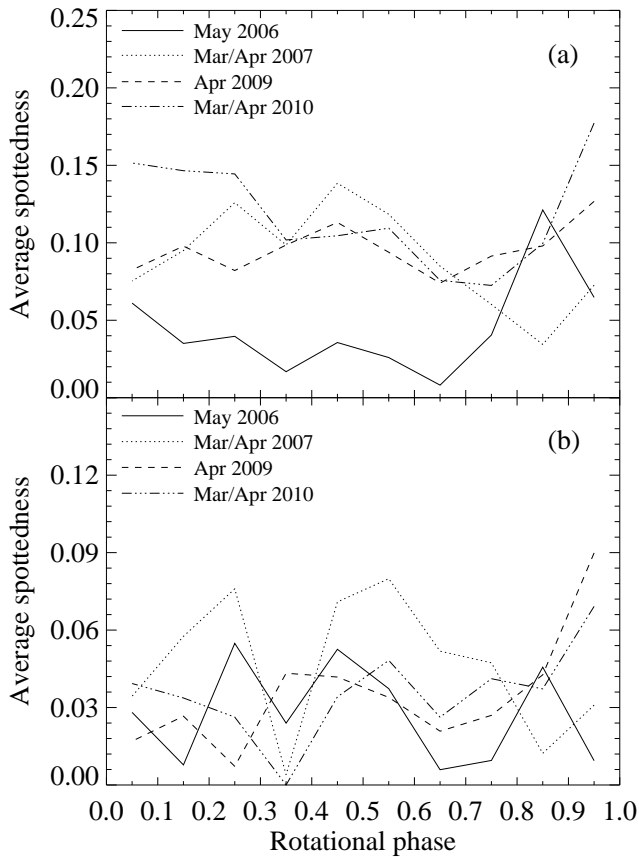


**Figure 11.** Average spottedness versus stellar rotational phase for HD141943, averaged over (a) 0° to +90° and (b) 0° to +60° latitude. The phase has been binned into 0.1 steps to remove any small scale variations.

that show this are often those that do not have well sampled observational phases (i.e. Fig. 13, Donati et al. 2003). In addition, preliminary observations of the late-F star HR 1817 (Marsden et al. 2006b), with a rotation period of ~1.0 d and a convective zone depth of ~0.17 R<sub>\*</sub>, have shown it to have a small, but intense, polar spot. A significantly larger sample size is required before any firm conclusions can be made about the relationship between polar spot size/intensity and

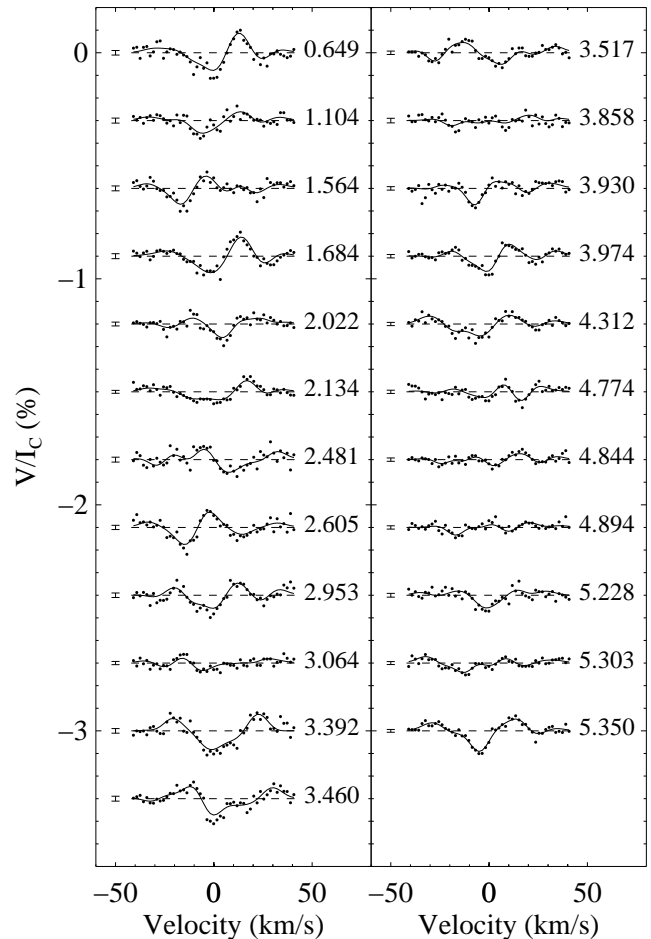


**Figure 12.** Maximum entropy fits for the Stokes V LSD profiles of HD 141943, March/April 2007. The dots represent the observed LSD profiles while the lines represent the fits to the profiles produced by the imaging code. Each profile is shifted down by 0.003 for graphical purposes. The rotational phases at which the observations took place are indicated to the right of each profile while the 1 $\sigma$  error bars are given to the left of each profile.

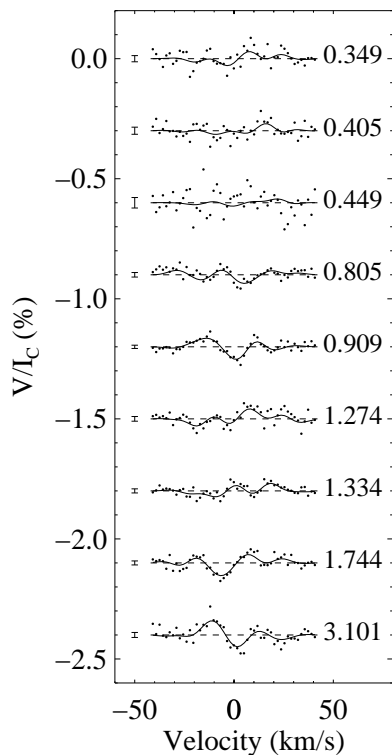


**Figure 13.** Maximum entropy fits for the Stokes V LSD profiles of HD 141943, April 2009. As explained in Fig. 12, the dots represent the observed LSD profiles while the lines represent the fits to the profiles produced by the imaging code.

basic stellar parameters. Indeed, given the possible variation in the size of the polar spot seen on LQ Hya (Donati et al. 2003) it may well be that young active stars go through cycles where the size of the polar spot varies as has been mentioned by Barnes (2005).

Granzer (2004) has used thin flux tube models to determine the latitude distribution of spot emergence for young rapidly-rotating stars. Although these models are based on a solar-like interface dynamo (which may not be applicable to such stars, see Section 5.2) it is still interesting to see how well the models compare to the results for HD 141943. Fig. 10 shows that at all 4 epochs HD 141943 has a peak in fractional spottedness around  $0^\circ$  to  $+40^\circ$  latitude, with another peak around  $+70^\circ$  to  $+85^\circ$ . For a PMS star of  $1.0 M_\odot$  the models of Granzer (2004) predict that the star should have a spot emergence distribution of between  $+30^\circ$  to  $+70^\circ$  latitude with a peak around  $+50^\circ$ . For a  $1.7 M_\odot$  PMS star this distribution is more spread out with a range from  $+20^\circ$  to  $+70^\circ$  with a peak around  $+30^\circ$  and  $+40^\circ$ . The distribution of fractional spottedness shown in Fig. 10 is not that dissimilar to the combination of the  $1.0 M_\odot$  and  $1.7 M_\odot$  distributions given by Granzer (2004) with the exception that the higher-latitude peak in spottedness is at a higher latitude in our images than predicted by the models. However, the models predict that for the more Zero-Age Main-Sequence (ZAMS) age stars, such as most of the other stars in Table 5, the latitude of peak distribution in spots is predicted to decrease, but the more intense polar spots of these stars would appear to indicate that this is not happening.

As suggested by Granzer (2004) and others, it is possible

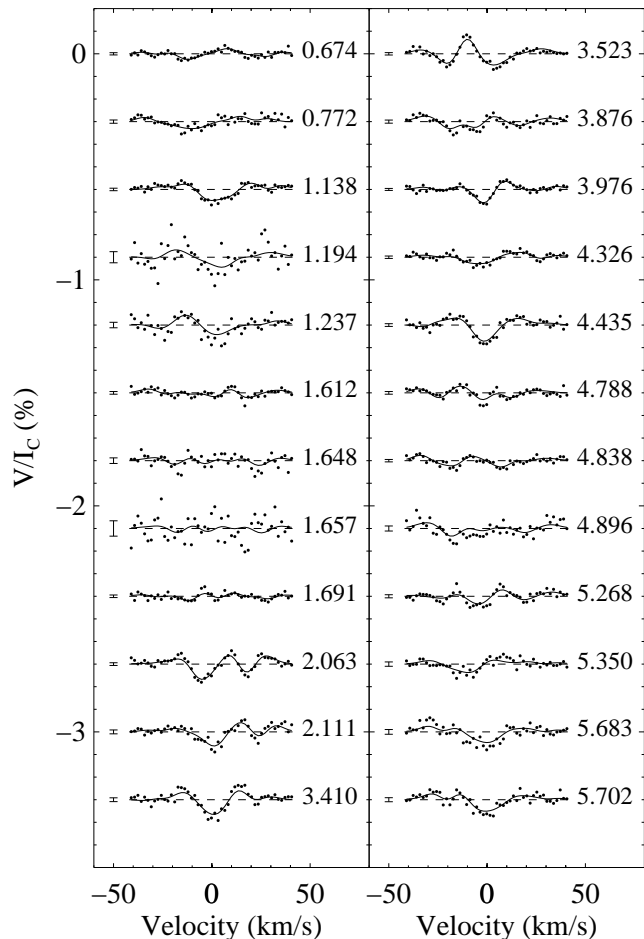


**Figure 14.** Maximum entropy fits for the Stokes V LSD profiles of HD 141943, March/April 2010. As explained in Fig. 12, the dots represent the observed LSD profiles while the lines represent the fits to the profiles produced by the imaging code.

a strong meridional flow is pushing most of the spots, which form at lower-latitudes, to the polar region, with stars with deeper convective zones possibly having stronger meridional flows and thus forming more intense polar spots. Such a mechanism might well explain the bimodal spot distribution seen in Fig. 10 with the lower peak in the distribution representing the latitude at which the flux tubes emerge and the polar spot those spots that have been driven to the poles by the meridional flow. Such a mechanism may also explain the non-uniform polar spots seen on a number of stars, if the polar spot is being formed by a number of smaller spot features. This is still just speculative, but Weber, Strassmeier & Washuettl (2005) have shown tentative evidence for large poleward meridional flows on early-K giants.

## 5.2 Large-scale magnetic topology

The maps of the large-scale magnetic topology on HD 141943 from three epochs (Fig. 3, Fig. 4 and Fig. 5) show that the radial field on HD 141943 had a mixed polarity at all latitudes for all epochs. The azimuthal field appears to be dominated by a ring of positive field around the pole

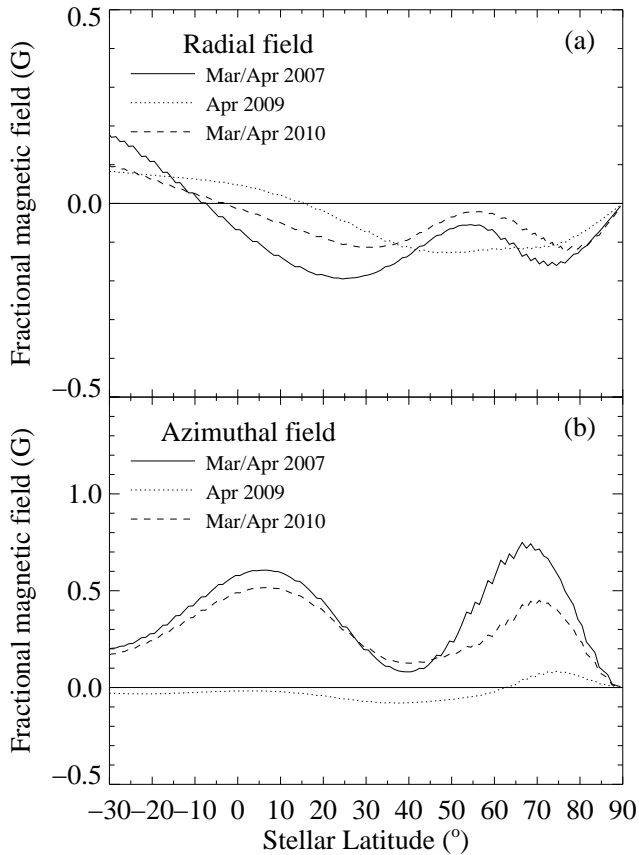


**Figure 16.** Fractional magnetic field for (a) the radial magnetic field and (b) the azimuthal magnetic field versus stellar latitude for HD141943. This is based on the absolute value of the magnetic field at each latitude and is defined by equation 2, with  $S(\theta)$  now representing the value of the magnetic field.

at all epochs, although the intensity of the polar ring is reduced in 2009. This is shown in the results from Table 4, which show that the toroidal field is predominately axisymmetric ( $\sim 70 - 75$  per cent) while the poloidal field is predominately non-axisymmetric ( $\sim 70 - 80$  per cent), with the ratio not appearing to change significantly between the three epochs. The other obvious feature of the azimuthal field is the increase in the amount of negative field on the stellar surface in the 2009 image compared to the 2007 and 2010 images. As these surface regions of radial and azimuthal field are believed to be the poloidal and toroidal components of the large-scale dynamo field, the latitudinal distribution and evolution of these regions are an important window onto the operation of the stellar magnetic dynamo.

There appears to be no large-scale magnetic polarity reversal on HD 141943 over the 3 years of observations. This is similar to the young early-G star HD 171488 (Marsden et al. 2006a; Jeffers & Donati 2008; Jeffers et al. 2010) and the young early-K stars AB Dor and LQ Hya (Donati et al. 2003) none of which have shown evidence of magnetic polarity reversals over several years of observations. In contrast, a magnetic polarity reversal has been seen on the mature Sun-like star HD 190771 (Petit et al. 2009) in 3 years of observations and the mature late-F star Tau Boo has shown two magnetic polarity reversals in the space of  $\sim 2$  years

(Donati et al. 2008; Fares et al. 2009). However, Tau Boo is host to a “Hot Jupiter” (Butler et al. 1997) that may be affecting the star’s magnetic cycle.

An axisymmetric field in the form of a ring of azimuthal field around the pole appears to be a common element of active solar-type stars with such a ring also seen on all reconstructed images of the young early-G stars HD 171488 (Marsden et al. 2006a; Jeffers & Donati 2008; Jeffers et al. 2010) and HD 106506 (Waite et al. 2010), as well as being seen on a number of images of the young early-K star AB Dor (Donati et al. 2003). Such a ring has also been seen on more evolved solar-type stars such as the early-G FK Com star HD 199178 (Petit et al. 2004b) and the early-K RSCVn star HR 1099 (Donati et al. 2003; Petit et al. 2004a). Such large-scale regions of azimuthal magnetic field near the surface of these active stars has led to the belief that such stars have a fundamentally different dynamo in operation than that of the solar-type interface-layer dynamo, as such regions should not be seen near the stellar surface if a solar dynamo were in action. It is thought that such stars contain a distributed dynamo, one that operates throughout the stellar convective zone rather than being restricted to the interface layer (see Donati et al. 2003).

Such a concept has recently been supported by theoretical models of Brown et al. (2010) which have shown that a stable magnetic dynamo can exist without an interface-layer. These models are based on a rapidly-rotating Sun (up to 3 times the current solar rotation rate) and also show large regions of near-surface “wreaths” of longitudinal magnetic field. These wreaths are similar to the rings of azimuthal field seen on active solar-type stars, except that they are at lower latitudes. Perhaps the higher Coriolis force experienced by the more rapidly rotating stars such as HD 141943 (rotating around 10 times the solar value) are pushing these wreaths to higher latitudes.

Table 4 shows that in all epochs both the poloidal and toroidal magnetic fields are very complex with over 50 per cent of the magnetic energy in orders higher than an octupole (except for the poloidal magnetic energy in 2009 which has only 45 per cent of the magnetic energy in orders higher than an octupole). There also appears to be evolution in the magnetic field between the epochs. In 2007 the magnetic energy is reasonably evenly balanced between poloidal and toroidal components (47 per cent to 52 per cent respectively) while in 2009 the poloidal field is extremely dominant (82 per cent to 17 per cent) and in 2010 the magnetic energy is again balanced between the poloidal and toroidal components (50 per cent in each). As explained in Section 4.2, the dataset in 2009 is significantly poorer than those in 2007 and 2010 and this may be having an influence on the reconstruction of the magnetic topology for this epoch. However, when we tried to reconstruct the magnetic topology for the 2007 and 2010 epochs using a small subset of the data similar to that of the 2009 dataset there was virtually no change in the ratio of poloidal and toroidal field. Thus we feel that the change in the poloidal/toroidal ratio seen in 2009 may well be real, but unfortunately we cannot prove this with any certainty.

Donati & Landstreet (2009) has looked at the changing magnetic field topologies on stars of different masses and rotation rates (see Fig. 3 in Donati & Landstreet 2009). This shows that stars around the mass and rotation rate of HD



141943 (actually preliminary results from the March/April 2007 dataset on HD 141943 are plotted in the figure) fall into an ‘active’ dynamo regime, which includes stars with Rossby number  $\lesssim 1$  and more massive than  $\sim 0.5 M_{\odot}$ . These stars produce predominantly non-axisymmetric poloidal magnetic field topologies as well as having significant amounts of toroidal field. At all three epochs studied in this paper HD 141943 does appear to have a predominantly non-axisymmetric poloidal field (and a predominantly axisymmetric toroidal field), but, as mentioned above, the ratio of poloidal to toroidal magnetic field appears to change for the 2009 epoch.

A change in the ratio of poloidal to toroidal magnetic field has been seen on another star. The previously mentioned mature late-F star Tau Boo (period  $\sim 3$  days) shows large changes in its ratio of poloidal/toroidal field during a magnetic cycle, with toroidal field dominating before a global polarity switch and poloidal field dominating after (Fares et al. 2009). This could indicate that the changes seen in the ratio of poloidal and toroidal field on HD 141943 are part of a stellar magnetic cycle on the star, however it would mean that it has undergone an extremely rapid evolution of its magnetic field, but has yet to undergo a magnetic polarity reversal. It would be useful to follow HD 141943 on at least yearly timescales to see whether the magnetic field does in fact undergo rapid magnetic evolution and polarity reversals, such as that evidenced by Tau Boo.

As part of the Sun’s magnetic cycle, the ratio of dipole to quadrupole components of the magnetic field changes. As can be seen in Table 4 there are significant changes in the percent of magnetic energy in dipole, quadrupole and octupole components for both the poloidal and toroidal fields. For example the per cent of poloidal magnetic energy in the dipole component changes from  $\sim 6$  per cent in 2007 to  $\sim 29$  per cent in 2009 and down to  $\sim 6$  per cent in 2010. The most significant changes appear to occur for the 2009 dataset. Assuming that the change seen in the magnetic topology of HD 141943 in 2009 is real, a comparison of the total magnetic energy (both poloidal and toroidal components) of HD 141943 appears to show that HD 141943 has also undergone a change in the complexity of its magnetic field from 2007 to 2009 and then back again in 2010. From Table 4 the total dipole component of the magnetic energy stays reasonably constant over all three epochs ( $\sim 24$  per cent in 2007,  $\sim 25$  per cent in 2009 and  $\sim 22$  per cent in 2010). The same can be said for the total octupole component ( $\sim 9$  per cent in 2007,  $\sim 7$  per cent in 2009 and  $\sim 12$  per cent in 2010). However, the total quadrupole component appears to change markedly in 2009 compared to the other two epochs ( $\sim 7$  per cent in 2007,  $\sim 18$  per cent in 2009 and  $\sim 9$  per cent in 2010) mostly due to an increase in the quadrupole component of the poloidal field. Now, as explained in Section 4.2 the poorer observations in 2009 may play a role in this change but this could be a change imparted by magnetic evolution on HD 141943.

## 6 CONCLUSIONS

HD 141943 is one of the youngest and most massive stars for which we have analysed the surface magnetic topologies for. For young stars it has the shallowest convective zone that we have yet studied. We have presented reconstructed

brightness (at 4 epochs) and magnetic (at 3 epochs) topologies of HD 141943. During the four year timebase of the brightness images the spot distribution on HD 141943 has changed very little with a smallish polar spot and a number of lower-latitude features at around  $0^{\circ}$  to  $+30^{\circ}$  latitude, seen at all epochs.

Over three years of observations the pattern of the magnetic topology of HD 141943 also looks at first glance to have experienced relatively little change, with positive and negative radial magnetic field seen at all latitudes and a ring of positive azimuthal magnetic field seen at all epochs. At all epochs the large-scale poloidal magnetic field of HD 141943 is mostly non-axisymmetric while the toroidal field is predominantly axisymmetric. The reconstructed magnetic topologies are rather complex with over 50 per cent of the magnetic energy in components higher than an octupole. When the magnetic images were analysed in more detail we found tentative evidence for a change in the magnetic field in 2009. The ratio of poloidal to toroidal field on HD 141943 goes from almost balanced in 2007 to being heavily dominated by poloidal magnetic field in 2009 and back to balanced in 2010. If real, this variation would indicate magnetic evolution on HD 141943.

## ACKNOWLEDGMENTS

The observations in this paper were obtained with the Anglo-Australian telescope. We would like to thank the technical staff of the Anglo-Australian Observatory (now the Australian Astronomical Observatory) for their, as usual, excellent assistance during these observations. We would also like to thank the anonymous referee who helped improve this paper. This project is supported by the Commonwealth of Australia under the International Science Linkages program.

## REFERENCES

- Baliunas S. L., Donahue R. A., Soon W. H., et al., 1995, *ApJ*, 438, 269
- Barnes J. R., Collier Cameron A., James D. J., Donati J.-F., 2000, *MNRAS*, 314, 162
- Barnes J. R., Collier Cameron A., James D. J., Donati J.-F., 2001a, *MNRAS*, 324, 231
- Barnes J. R., Collier Cameron A., James D. J., Steeghs D., 2001b, *MNRAS*, 326, 1057
- Barnes J. R., 2005, *MNRAS*, 364, 137
- Berdyugina S. V., 2005, *Starspots: A Key to the Stellar Dynamo*, *Living Rev. Solar Phys.* 2, (2005), 8. URL (cited on 2010 January 22): <http://www.livingreviews.org/lrsp-2005-8>
- Berdyugina S. V., Tuominen I., 1998, *A&A*, 336, L25
- Brandenburg A., 2005, *ApJ*, 625, 539
- Brown B. P., Browning M. K., Brun A. S., Miesch M. S., Toorme J., 2010, *ApJ*, 711, 424
- Brown S. F., Donati J.-F., Rees D. E., Semel M., 1991, *A&A*, 250, 463
- Browning M. K., 2008, *ApJ*, 676, 1262
- Butler R. P., Marcy G. W., Williams E., Hauser H., Shirts P., 1997, *ApJ*, 474, L115

- Charbonneau P., 2005, *Dynamo Models of the Solar Cycle*, *Living Rev. Solar Phys.* 2, (2005), 2. URL (cited on 2010 August 19): <http://www.livingreviews.org/lrsp-2005-2>
- Collier Cameron A., 1992, in Byrne P. B., Mullan D. J., eds, *Lecture Notes in Physics*, Vol. 397, *Surface Inhomogeneities on Late-Type Stars*, Springer, Berlin, p. 33
- Cutispoto G., Pastori L., Tagliaferri G., Messina S., Pallavicini R., 1999, *A&AS*, 138, 87
- Cutispoto G., Pastori L., Pasquini L., de Medeiros J. R., Tagliaferri G., Anderson J., 2002, *A&A*, 384, 491
- Cutispoto G., Tagliaferri G., de Medeiros J. R., Pastori L., Pasquini L., Anderson J., 2003, *A&A*, 397, 987
- Donati J.-F., Brown S. F., Semel M., Rees D. E., Dempsey R. C., Matthews J. M., Henry G. W., Hall D. S., 1992, *A&A*, 265, 682
- Donati J.-F., Collier Cameron A., 1997, *MNRAS*, 291, 1
- Donati J.-F., Brown S. F., 1997, *A&A*, 326, 1135
- Donati J.-F., Semel M., Carter B. D., Rees D. E., Cameron A. C., 1997, *MNRAS*, 291, 658
- Donati J.-F., 1999, *MNRAS*, 302, 457
- Donati J.-F., Collier Cameron A., Hussain G., Semel M., 1999, *MNRAS*, 302, 437
- Donati J.-F., Mengel M., Carter B. D., Marsden S., Collier Cameron A., Wichmann R., 2000, *MNRAS*, 316, 699
- Donati J.-F., Collier Cameron A., Semel M., et al., 2003, *MNRAS*, 345, 1145
- Donati J.-F., Howarth I. D., Jardine M. M., et al., 2006, *MNRAS*, 370, 629
- Donati J.-F., Moutou C., Farès R., et al. 2008, *MNRAS*, 385, 1179
- Donati J.-F., Landstreet J. D., 2009, *ARA&A*, 47, 333
- Dunstone H. J., Hussain G. A. J., Collier Cameron A., Marsden S. C., Jardine M., Stempels H. C., Ramirez Vlez J. C., Donati J.-F., 2008, *MNRAS*, 387, 481
- Fares R., Donati J.-F., Moutou C., et al., 2009, *MNRAS*, 398, 1383
- Granzer Th. Schüssler M., Caligari P., Strassmeier K. G., 2000, *A&A*, 355, 1087
- Granzer T., 2004, *Astron. Nachr.*, 325, 417
- Hillenbrand L. A., Carpenter J. M., Kim J. S., et al., 2008, *ApJ*, 677, 630
- Järvinen S. P., Berdyugina S. V., Tuominen I., Cutispoto G., Bos M., 2005, *A&A*, 432, 657
- Jeffers S. V., Donati J.-F., 2008, *MNRAS*, 390, 635
- Jeffers S. V., Donati J.-F., Alecian E., Marsden S. C., 2010, *MNRAS*, accepted
- Kochukhov O., Makaganiuk V., Piskunov N., 2010, *A&A*, 524, A5
- Kurucz R. L., 1993, CDROM #13 (ATLAS9 atmospheric models) and CDROM #18 (ATLAS9 and SYNTHES routines, spectral line database)
- Mackay D. H., Jardine M., Collier Cameron A., Donati J.-F., Hussain G. A. J., 2004, *MNRAS*, 354, 737
- Marsden S. C., Carter B. D., Donati J.-F., 2005a, in Favata F., Hussain G. A. J., Battrick B., eds. *Proceedings of the 13<sup>th</sup> Cambridge Workshop on Cool Stars, Stellar Systems and the Sun*, ESA Special Publications, Vol. 560, ESA, Noordwijk, The Netherlands, p. 799
- Marsden S. C., Waite I. A., Carter B. D., Donati J.-F., 2005b, *MNRAS*, 359, 711
- Marsden S. C., Donati J.-F., Semel M., Petit P., Carter B. D., 2006a, *MNRAS*, 370, 468
- Marsden S. C., Mengel M. W., Donati J.-F., Carter B. D., Semel M., Petit P., 2006b, in Casini R., Lites B. W., eds. *Proceedings of the 4<sup>th</sup> Solar Polarization workshop*, ASP Conference Series, Vol. 358, ASP, San Francisco, USA, p. 401
- Marsden S. C., Jeffers S. V., Donati J.-F., Mengel M. W., Waite I. A., Carter B. D., 2010a, in Kosovichev A., Rozelot J.-P., Andrei A., eds., *Proceedings of IAU Symposium 264, Solar and Stellar Variability: Impact on Earth and Planets*, Cambridge University Press, Cambridge, UK, p. 130
- Marsden S. C., Jardine M. M., Ramírez V'elez J. C., et al., 2010b, *MNRAS*, accepted (Paper II)
- Mengel M., 2006, Mphil thesis, University of Southern Queensland, Toowoomba, Queensland, Australia
- Nordström B., Mayor M., Andersen J., et al., 2004, *A&A*, 418, 989
- Parker E. N., 1993, *ApJ*, 408, 707
- Petit P., Donati J.-F., Wade G. A., et al., 2004a, *MNRAS*, 348, 1175
- Petit P., Donati J.-F., Oliveira J. M., et al., 2004b, *MNRAS*, 351, 826
- Petit P., Dintrans B., Solanki S. K., et al., 2008, *MNRAS*, 388, 80
- Petit P., Dintrans B., Morgenthaler A., Van Grootel V., Morin J., Lanoux J., Aurière M., Konstantinova-Antova R., 2009, *A&A*, 508, L9
- Randich S., 2001, *A&A*, 377, 512
- Schüssler M., Caligari P., Ferriz-Mas A., Solanki S. K., Stix M., 1996, *A&A*, 314, 503
- Semel M., 1989, *A&A*, 225, 456
- Semel M., Donati J.-F., Rees D. E., 1993, *A&A*, 278, 231
- Siess L., Dufour E., Forestini M., 2000, *A&A*, 358, 593
- Skilling J., Bryan R. K., 1984, *MNRAS*, 211, 111
- Strassmeier K. G., Pichler T., Weber M., Granzer T., 2003, *A&A*, 411, 595
- Unruh Y. C., Collier Cameron A., 1995, *MNRAS*, 273, 1
- Waite I. A., Carter B. D., Marsden S. C., Mengel M. W., 2005, *PASA*, 22, 29
- Waite I. A., Marsden S.C., Carter B.D., et al., 2010, *MNRAS*, accepted
- Weber M., Strassmeier K. G., Washuettl A., 2005, *Astron. Nachr.*, 326, 287
- Wichmann R., Krautter J., Covino E., Alcalá J. M., Neuhäuser R., Schmitt J. H. M. M., 1997, *A&A*, 320, 185